SOLDER CREEP-FATIGUE INTERACTIONS WITH FLEXIBLE LEADED PARTS

R. G. Ross, Jr.

L.C. Wen

April 1992

Draft chapter of book

Thermal Stress and Strain in Microelectronics Packaging

John H. Lau, Editor

Van Nostrand Reinhold, New York

SOLDER CREEP-FATIGUE INTERACTIONS WITH FLEXIBLE LEADED PARTS

R.G. Ross, Jr. and L.C. Wen

I. INTRODUCTION

In most electronic packaging applications it is not a single high stress event that breaks a component solder joint; rather it is repeated or prolonged load applications that result in fatigue or creep failure of the solder. The principal strain in solder joints is caused by differential expansion between the part and its mounting environment due to changes in temperature (thermal cycles) and/or due to temperature gradients between the part and the board.

The function of strain relief elements -- such as the flexible metal leads of the electronic components -- is to lower the differential-expansion induced loads (stresses) on the solder joints to levels well below the solder yield strength, thus significantly reducing the generation of plastic strain. By reducing the developed strain, flexible leads greatly enhance solder joint reliability. Figure 1-1 illustrates a variety of flexible leads common to surface-mount electronic parts.

While flexible leads invariably increase the reliability of soldered electrical connections, the level or amount of improvement varies widely with the specific application. This variability stems from the fact that the elastic spring properties of the leads that reduce the load also prolong the load on the solder. Prolonging the load over long time spans raises the specter of time-dependent failure mechanisms involving phenomina such as creep, corrosion, and long-term metallurgical changes. Creep strain is probably the most important time-dependent damage accrual mechanism; under typical multi-hour loading conditions the solder joints of flexible leaded parts can be expected to undergo significant levels of strain due to creep of the solder in response to the applied elastic forces from the strain relief elements. This creep-induced strain has the same damaging effect as more immediately induced plastic strain, and must be summed with the plastic strain to achieve the total plastic strain that is correlated with fatigue life.

Because of creep effects, the total strain range during any given loading cycle can be a strong function of solder temperature, the loading time per cycle, the applied solder stress, and the spring constant of the strain relief elements. The implication is that creep related strain--and in particular the time, temperature, and stress dependency of creep--must be carefully factored into the design and testing of flexible leaded parts.

Although extensive research in recent years has led to an increasingly mature understanding of the creep-fatigue properties of solder as an engineering material, much less headway has been made in quantifying solder creep-fatigue behavior at the electronic package systems level. The objective of this chapter is to explore the complex systems-level creep-fatigue interactions involved in electronic part solder joints, and in particular to illustrate the key solder-joint structural configuration and environmental stress

Draft chapter of book
Thermal Stress and Strain in Microelectronics Packaging
John H. Lau, Editor
Van Nostrand Reinhold, New York, 1W2

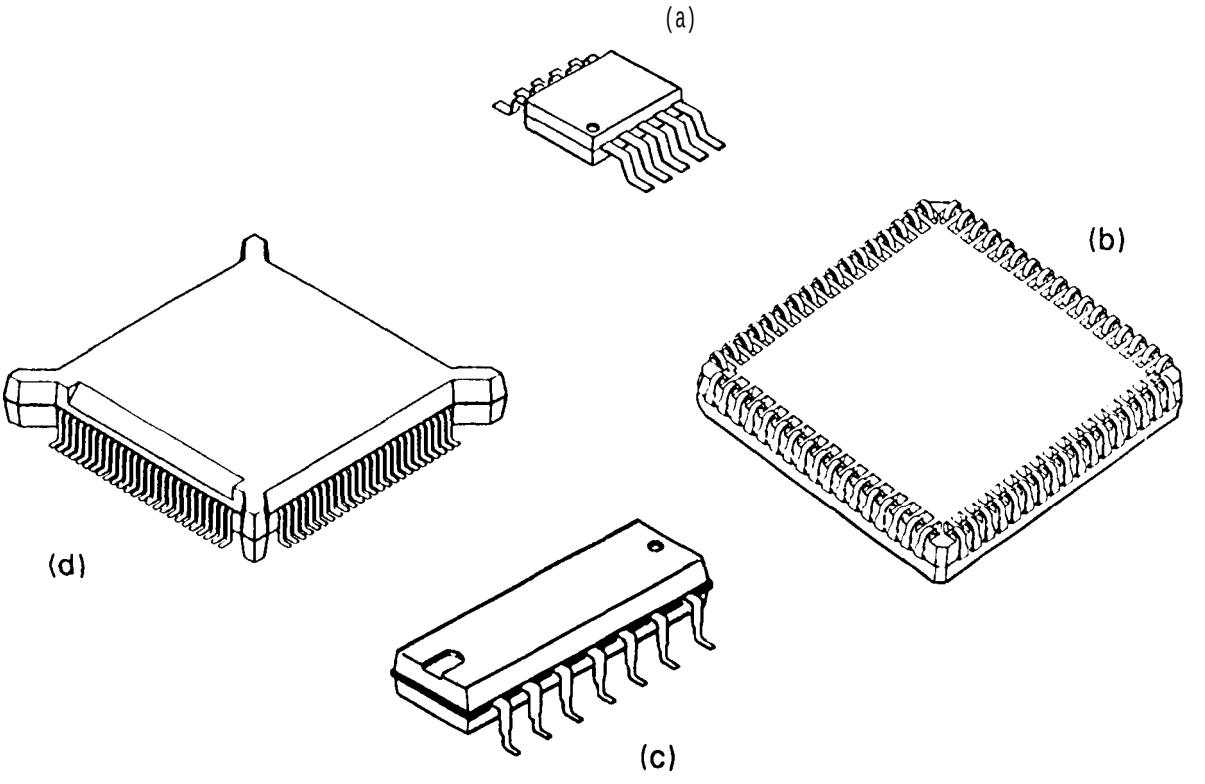

Fig. 1-1. Typical flexible lead geometries found on surface-mount electronic components: (a) Flat-pak with gull-wing leads, (b) Plastic leaded chip carrier (PLCC) with J-leads, (c) DIP with gull-wing leads, and (d) Quad Flat-pak with fine-pitch gull-wing leads.

dependencies. Important issues include the effects of component lead flexibility, operating temperature, thermal cycling depth, and cyclic frequency of loading. Understanding these issues is important to both achieving robust electronic packaging designs that meet the end-use requirements, and to defining and interpreting appropriate accelerated testing procedures for hardware qualification.

Chapter Organization

The chapter begins by first reviewing the Coffin-Manson fatigue-life relationships that highlight the importance of repeated plastic strain--including creep strain--in determining the useful life of solder joints. Next, the fundamental parameters controlling creep in solder are examined together with the constitutive models that capture the parameter dependencies in mathematical terms. Combining these constitutive models with non-linear finite element modeling techniques provides one of the best means of computing and studying the creep-fatigue behavior of solder in complex flexible-lead loading conditions. One such model, developed by the authors [1,2], will be used extensively throughout the chapter to explore the role of lead flexibility in both isothermal mechanical cycling and thermal cycling environments. Mechanical cycling with flexible leaded parts will be shown to introduce strong dependencies on the rate of cycling and the temperature of the solder. Thermal cycling will be shown to additionally introduce unidirectional creep-ratcheting that can cause parts to climb out of the solder or into the solder normal to the loading direction; failure models based on the Coffin-Manson fatigue life relationships will be examined and used to interpret the relative importance of combined creep-fatigue and creep-ratcheting mechanisms. The chapter ends with a summary of the diverse issues surrounding creep-fatigue interactions with flexible leaded parts.

II. MODELING OF SOLDER CREEP-FATIGUE INTERACTIONS

The most important cause of solder joint failure is repeated straining during temperature cycling as a result of mismatch of the Coefficients of Thermal Expansions (CTE) of the electronic part-lead assembly and the substrate to which it is soldered.

The fatigue-dominated process, often referred to as low-cycle fatigue, is characterized by a large plastic strain range and is generally modelled by a Coffin-Manson type relationship modified to account for any creep strain and its dependence on cycle frequency and temperature. Lau [3] and Frear [4] provide extensive reviews of the literature in this area.

Figure 2-1 shows representative fatigue-life data for 63-37 Sn-Pb near-eutectic solder [5,6,7]. The plot illustrates the typical logarithmic dependency between cycles-to-failure and the level of plastic strain range. The data can be fitted to the empirical Coffin-Manson relationship [8,9]:

$$N_f^{\beta} \Delta\epsilon = C \qquad (1)$$

where

N_f = number of cycles to failure
$\Delta\epsilon$ = cyclic plastic strain range
β ≈ 0.40 (from curve slope in Fig. 2-1)
C ≈ 0.80 (for 50% solder failure limit in Fig. 2-1)

Although the intercept C varies somewhat for various alloys, the slope β has been found to be around 0.5 for most ductile metals including solder, aluminum, copper, and stainless steel [5]. However, β has been found to vary modestly with the degree of damage used to define failure [10,11]. Lower levels of damage, such as "cycles to 50% load reduction for a constant strain", tend to yield steeper Coffin-Manson slopes; on the other hand, higher levels of damage, such as complete separation of the solder joint, tend toward lower β values. This trend is illustrated in Figure 2-2.

A flatter slope ($\beta \approx 0.40$) is used in this chapter as more representative of the dependence of the number of cycles required to achieve total joint separation, and thus an electrical open circuit.

Use of Coffin-Manson Relationships to Account for Creep Strain

The Coffin-Manson relationship (Equation 1) can be used for life prediction with flexible leaded parts only if the strain used is the total plastic strain including creep strain. This requires that the creep strain be accurately determined and added to any immediately produced plastic strain.

In practice, experimentally or analytically determining the creep strain can be exceedingly difficult to do; this has led to empirical modification of the Coffin-Manson equations to indirectly include the contribution of creep strain likely to occur, and its dependence on cycle rate and temperature. The

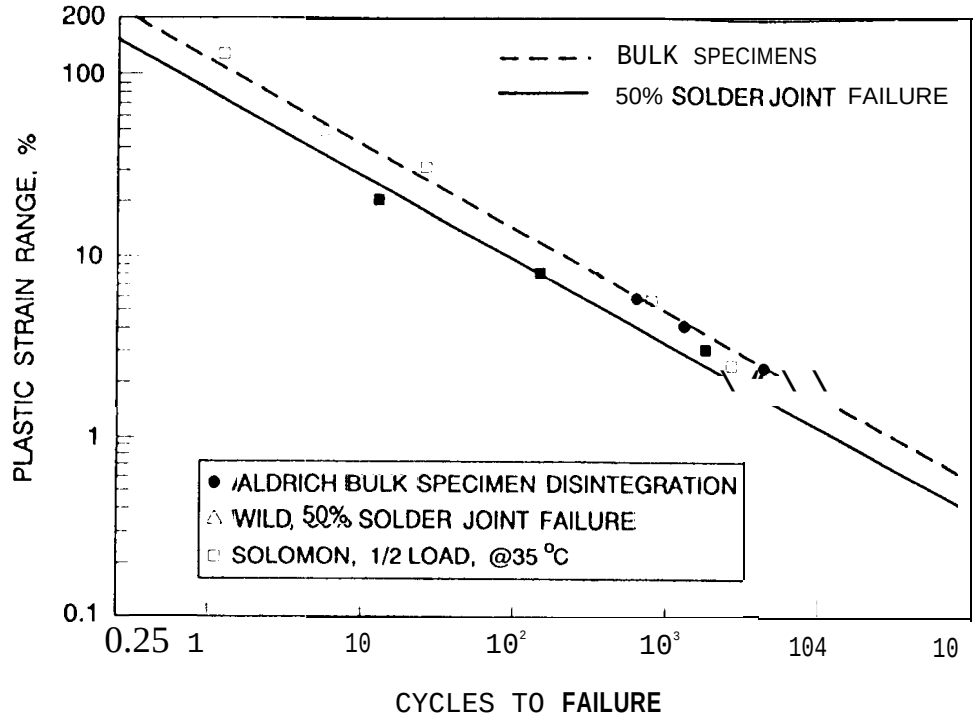

Fig. 2-1. Coffin-Manson curves fitted to typical eutectic Sn-Pb solder fatigue data from Aldrich [5], Wild [6], and Solomon [7].

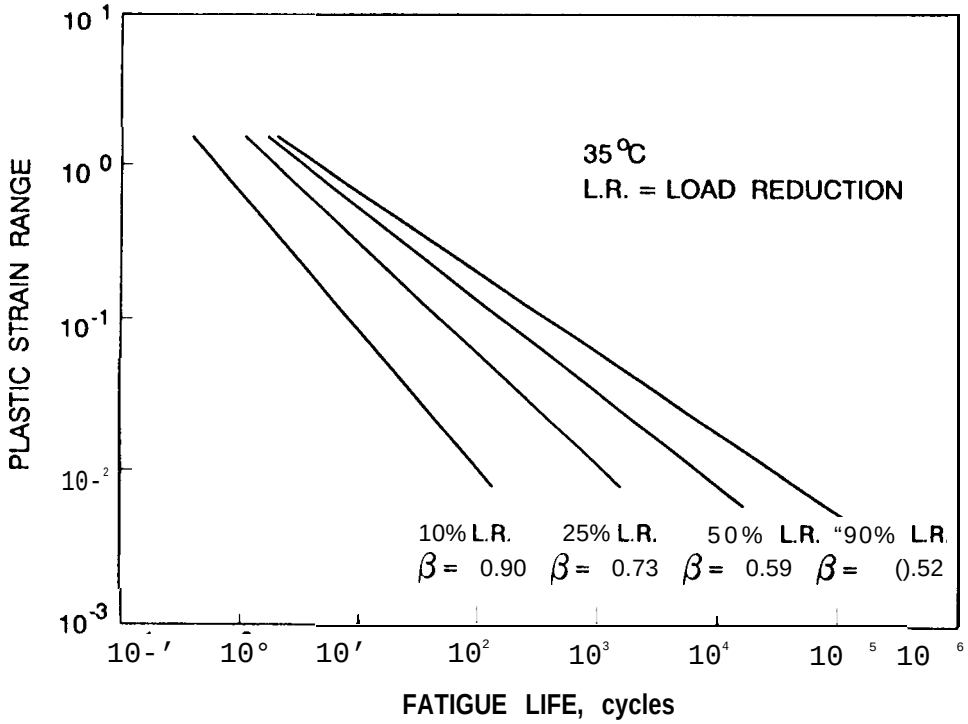

Fig. 2-2. Effect of definition-of-failure on slope of Coffin-Manson fatigue curves (from Solomon [11]).

simplest of the frequency-modified Coffin-Manson relationships [12,13] is of the form:

$$N_f^{\beta} \Delta\epsilon \, f^m = C \qquad (2)$$

where (f) is the frequency of applied loading and (m) is a design-specific, temperature-dependent material parameter. Solving explicitly for cycle life gives

$$N_f = \left[\frac{C}{\Delta\epsilon \, f^m} \right]^{1/\beta} \qquad (3)$$

To obtain a quantitative feel for the value of the frequency exponent (m) it is useful to compare Equation 3 to representative frequency-dependence data. Fitting Equation 3 to the low-frequency portion of the data shown in Figure 2-3 [10,14,15] gives

$$N_f \propto f^{-m/\beta} \approx f$$

This corresponds to $m = -\beta \approx -0.4$. In contrast, at frequencies above 0.1 cycle/minute, fatigue life for this loading system is seen to become much less sensitive to frequency as creep strain becomes small relative to other time-independent strain mechanisms. Thus the value of m varies from around -0,4 to zero over the range of frequencies tested.

Although Equation 2 recognizes the strong time dependence of creep strain, its simple form is unable to capture the important interrelationships between frequency, temperature, lead stiffness, and other parameters known to also have strong influences on generated strain. This limits its applicability to a specific design for which the equation has been calibrated. The m = -0.4 value derived above may therefore be of limited use for the prediction of performance of solder-joint systems significantly different from those used to gather the data in Figure 2-3.

To help correct for this important weakness, Engelmaier [16,17,18] has developed a more complete fatigue life relationship that explicitly accounts for lead stiffness and other parameters such as cyclic loading rate and solder and substrate temperature. Engelmaier's modified version of the Coffin-Manson equation is of the form:

$$N_f = \left(\frac{C \, A \, h}{K \, \Delta X^2} \right)^{1/\beta} \qquad (4)$$

where:

- c = constant
- N_f = mean cycles to fatigue failure
- K = stiffness of part lead in direction of loading (lb/in)
- A = effective solder joint loading area (in^2)
- AX = lead displacement range = $x(\alpha_p \Delta T_p - \alpha_b \Delta T_b)$ (inches)
- x = distance from part center to corner lead (inches)
- α_p = CTE of part-lead, ("C-l)

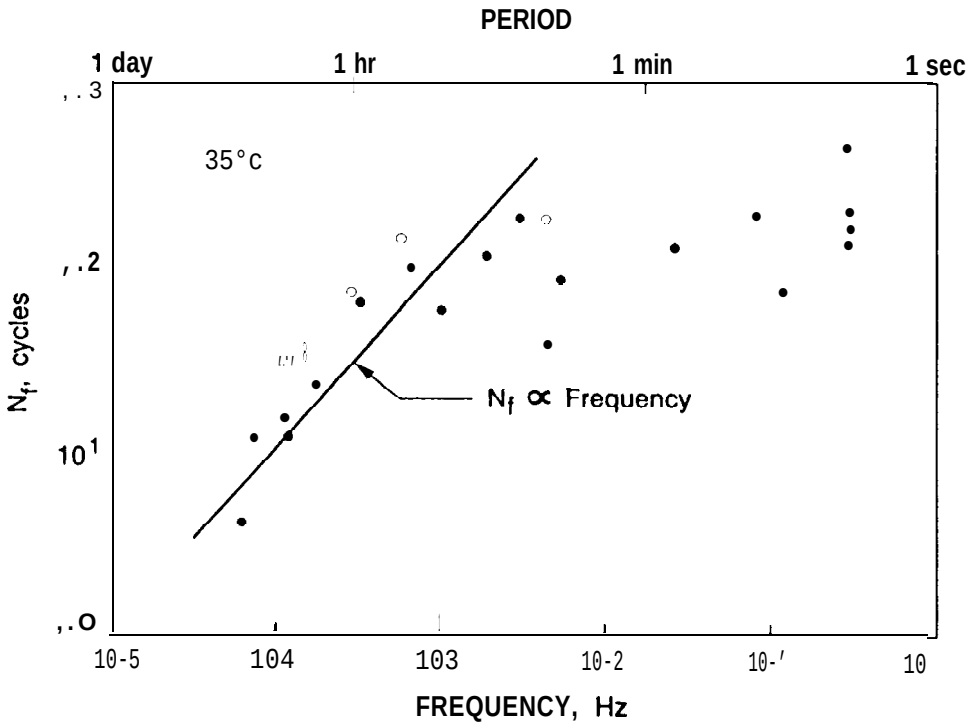

Fig, 2-3. Dependence of fatigue life of 60-40 Sn-Pb solder on loading frequency as measured by various investigators [10,14,15].

α_b = CTE of substrate board, ("C-l)
ΔT_p = ΔTemperature of part, °C
ΔT_b = ΔTemperature of board, "C
h = solder joint effective height, inches
β = 0.442 + 6.0x10^{-4} T_m - 0.0174 ln(1 + 360/τ)
T_m = mean solder Temperature, 'C
τ = half-cycle dwell time, minutes

Equation 4 is equivalent to saying that the strain range in the Coffin-Manson relationship (Equation 1) is given by

$$\Delta\epsilon \propto \left[\frac{K\,\Delta X^2}{A\,h}\right] \qquad (5)$$

Equation 5 suggests an approximately linear relationship between strain range and lead stiffness (K), and a squared dependency on lead deflection range (AX). Note that cyclic frequency of loading is not explicitly dealt with; rather half-cycle dwell time (τ), which is the more relevant parameter for creep, is incorporated as a variation in the Coffin-Manson slope β. Varying τ from 1 minute to 10 minutes causes β to vary from 0.354 to 0.394. To understand this change consider a system exhibiting N_1 = 1000 cycles to failure with τ = 1 minute. If all other parameters remain constant, the reduction (N_2/N_1) in the cycles-to-failure when τ is increased to 10 minutes can be computed by noting that

$$N_1^{\beta_1} = N_2^{\beta_2}$$

thus

$$N_2/N_1 = N_1^{(\beta_1/\beta_2 - 1)} \qquad (6)$$

This change in β can also be converted to an equivalent change in strain range by noting that

$$N_1^{\beta}\,\Delta\epsilon_1 = N_2^{\beta}\,\Delta\epsilon_2$$

thus

$$\Delta\epsilon_2/\Delta\epsilon_1 = (N_2/N_1)^{-\beta} \qquad (7)$$

For our example of a 10x change in dwell time, Equations 6 and 7 give

$$N_2/N_1 = (1000)^{(0.354/0.394 - 1)} = 0.496$$

and

$$\Delta\epsilon_2/\Delta\epsilon_1 = (0.496)^{-0.39} = 1.31$$

Thus the cycles to failure are reduced from 1000 to 496 by increasing the dwell time from 1 minute to 10 minutes. This is seen to also correspond to roughly a 30% increase in the strain range. To compare these results to the predictions of Equation 3, one can assume that the 10x increase in dwell time corresponds to a 10x reduction in frequency; thus, from Equation 3

$$N_2/N_1 = (f_2/f_1)^{-m/\beta} = (0.1)^{1.0} = 0.1$$

This is a considerably larger change than predicted by Engelmaier's relationship, and is indicative of the difficulty in extrapolating data from one set of test conditions to another. Understanding the issues underlying these difficulties is an important objective of the remaining sections of this chapter,

As a final step in examining the solder strain dependencies implied by Engelmaier's equation, one can examine the sensitivity of fatigue life to solder temperature. Like loading dwell time, mean solder temperature (T_m) is incorporated into Equation 4 as a variation in the Coffin-Manson slope β. For 20°C and 30°C solder temperatures and a ten-minute dwell time, we obtain β values of 0.39117 and 0.39717, respectively, Substituting these into Equations 6 and 7 gives

$$N_2/N_1 = (1000)^{(0.39117/0.39717 - 1)} = 0.90$$

and therefore

$$\Delta\epsilon_2/\Delta\epsilon_1 = (N_2/N_1)^{-\beta} = (0.9)^{-0.39} = 1.04$$

This implies that a 10"C increase in temperature causes a 4% increase in strain range and a corresponding 10% reduction in fatigue life.

Although Engelmaier's equation has considerably greater applicability than the original freciuencY-compensated Coffin-Manson equation, a remainina weakness in Equation 4 ·s the- fact' that the influences of temperature, lead stiffness, dwell time, and deflection range are treated as independent of one another. We will see later in this chapter that the interdependence is, in fact, very strong; for example, the influence of temperature on solder creep strain with highly flex ble leads is very different from the temperature dependence with stiff leads (LCC parts). To explore these issues in greater depth we must turn to more elaborate and comprehensive modeling approaches.

Solder Constitutive Relationships

As an alternative to the modified Coffin-Manson equations of Engelmaier and others, recent research has turned toward computing the plastic and creep strain dependencies on applied loads and temperatures using special non-linear finite element creep simulation models [1,2,19]. The finite element programs make use of the fundamental constitutive equations that model the dependency of solder strain rate on applied stress, temperature, and metallurgical properties. This has the advantage of accurately including the stiffness and geometry of the entire part-lead-substrate system, spatial detail within the solder joint itself, as well as the measured metallurgical properties of solder.

Figures 2-4 and 2-5 summarize representative data for the creep properties of solder [20-26]; an extensive review of these data is presented by Arrowood, et al. [27]. Figures 2-4 and 2-5 highlight the strong sensitivity of strain rate to solder age and metallurgical history and the strong Arrhenius dependency on temperature. Notice that solder exhibits three distinct strain-rate slope behaviors depending on the stress and temperature level. Regions I and III are regions of classic metal plastic deformation, whereas Region 11 is a so-

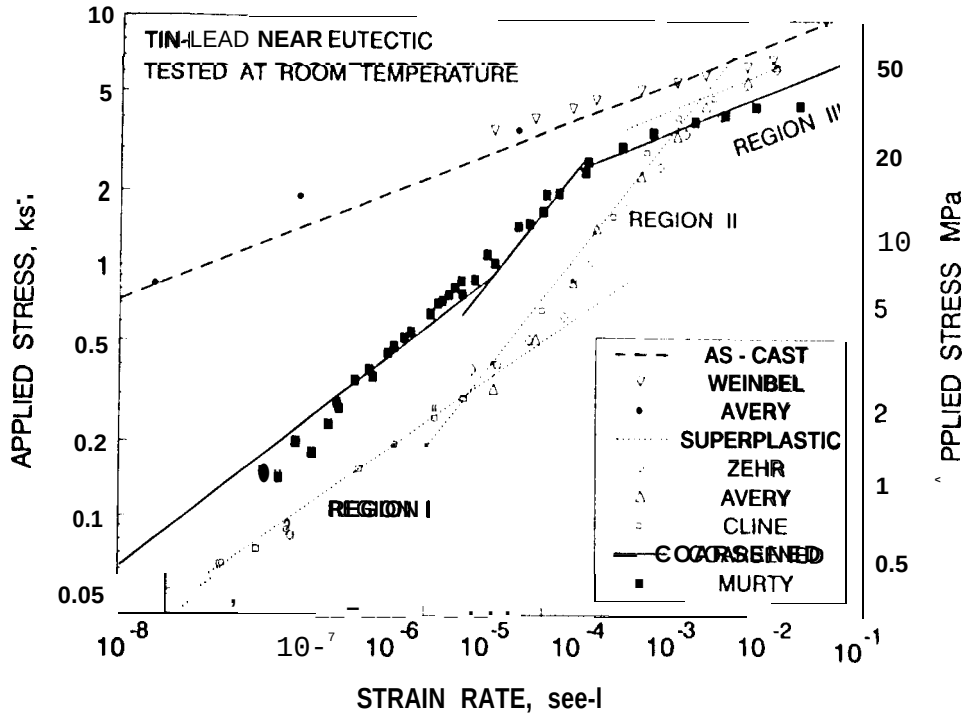

Fig. 2-4, Dependence of strain-rate on applied stress and metallurgical condition of room-temperature eutectic Sn-Pb solder.

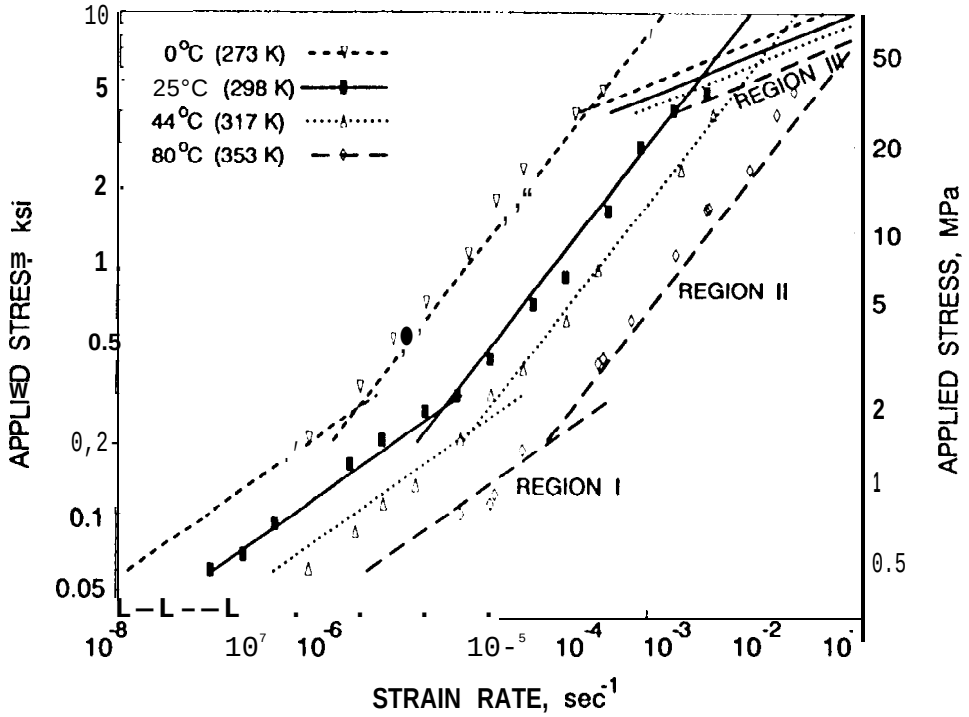

Fig. 2-5. Dependence of strain-rate on applied stress and temperature for eutectic Sn-Pb solder (from Cline and Alden [20]).

called region of superplastic behavior. In this superplastic region the solder is able to withstand much larger levels of deformation without rupture. Within each region the creep behavior of solder is well approximated by [27]:

$$\dot{\varepsilon} \propto \sigma^n g^{-p} \exp(-Q/kT) \cong \sigma^n g^{-p} \xi^{(T/10)} \quad (8)$$

where:

$\dot{\varepsilon}$ = solder strain rate, sec^{-1}
σ = solder stress
n = creep exponent (typically n = 2 to 3)
g = grain size
p = grain size exponent (typically p = 1.6 to 2.3)
Q = thermal activation energy of creep
ξ = temperature dependence per $10^{\circ}K$ (typically ξ = 1.5 to 2)
T = solder temperature (°K)
k = Boltzmann constant

Note in Figure 2-4 that "as-cast" solder has been found to have extremely high creep resistance when compared to fine-grain "superplastic" solder; similarly, larger-grained "coarsened" solder, generally the result of prolonged aging or thermal processing, has been found to be intermediate in creep resistance, With respect to the "as-cast" solder, Arrowood, et al. [27] have observed that the much greater creep resistance reported for this solder may be caused by the highly banded Pb-Sn lamellae structure often encountered with slowly cooled cast solder joints. If so, this high level of creep resistance may not be relevant to small rapidly cooled electronic component solder joints, which rarely exhibit banded solder structures.

In contrast to the anomalously low creep rate of "as-cast" solder, "superplastic" solder exhibits a much higher creep rate and tolerance to plastic deformation; this superplastic behavior is often associated with fine uniformly distributed grain structures similar to those found in electronic solder joints that are relatively small and have solidified rapidly from the melt (see Figure 2-6). Because high creep rate correlates with increased strain with flexible leaded parts, prudence demands that the high-creep-rate behavior of superplastic solder be carefully considered when dealing with flexible leaded parts.

When solder undergoes long-term aging of a year or more, or is thermally processed, the grain size of the solder grows as shown in Figure 2-6 [2,28]. We refer to this solder as "coarsened solder". Of the three solder structures, coarsened solder is probably the most representative of aged solder joints in real electronics applications. The increased grain size of coarsened solder restricts creep strain and thus makes it more resistant to failure under creep loading conditions [25,26]. Because of the significant variability between "superplastic" solder and "coarsened" (larger-grain) solder, the properties of both will be treated parametrically in later sections of this chapter.

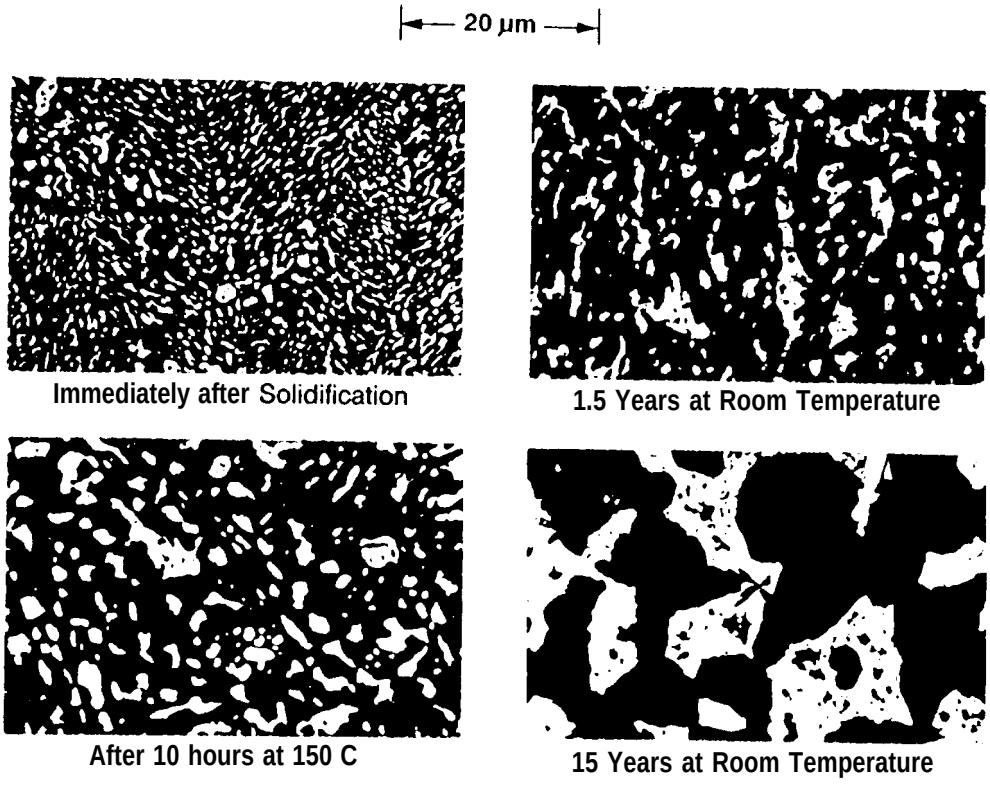

Fig. 2-6. SEM back-scatter photographs (tin is dark region) showing cross-sections of typical gull-wing flat-pak solder joints taken from spacecraft electronics with the indicated aging histories (From Ross, et al. [2]).

Finite Element Creep-Fatigue Modeling

Given a time history of environmental loading (e.g., electronic package temperature vs. time), a finite-element creep simulation program uses the constitutive properties of solder, such as those in Figure 2-5, to compute the resulting strain in each element of the solder joint as a function of the applied stress over time Varying the system geometry, cycle rate, thermal cycle depth, or any of a wide variety of parameters, allows the resulting effects on solder strain history to be observed directly.

In operation, a finite-e" ement creep-simulation program divides the time response of the solder joint into thousands of tiny-time increments; for each time increment the solder's incremental plastic stain response is computed based on the stress existing in the solder and the solder's temperature. One common approach is to start each time increment by computing the instantaneous stress in each solder element using a classical finite element elastic structural model of the complete part-l ead-solder-PWB system. The forcing function for the stresses is the instantaneous geometry of the package system, including previously accrued plastic deformation of the solder elements together with lead deflections applied externally by thermal-cycle differential expansions or mechanical (isothermal) cycling. Following computation of the stress, the above-described constitutive equations for solder are used together with the current solder temperature to compute the plastic stain rate in each solder element, and thus the solder incremental strain during the time interval.

Some programs continuously adjust the size of the time increment to insure near-constant strain-rate during any given time increment. This is desirable to prevent strain integration errors and model instabilities caused by excessive stress relaxation during any time interval. In general, simulations of multi-hour loading cycles representative of typical electronics applications involve time steps ranging from 0.001 seconds to 1 minute, thus leading to as many as 1 million strain-increment solutions per simulation run. The shortest time increments are generally required during periods of elevated temperature where stress relaxation occurs rapidly.

Because of the heavy computational load presented by creep-simulation algorithms, the finite element description of the solder system often has to be carefully simplified to preserve the important structural and constitutive features of the solder system while sacrificing non-critical detail. Example finite-element creep-fatigue simulation runs are used throughout the remainder of this chapter to further explore the nature of flexible leaded parts and to contrast the results with the modified Coffin-Manson equations described earlier.

III. ROLE OF LEAD STIFFNESS IN ISOTHERMAL LOADING

It is clear from the constitutive relationships in Figures 2-4 and 2-5 that applied stress, solder metallurgical structure, and temperature strongly influence the strain developed in solder during an application loading condition. As previously pointed out, a key function of flexible leads is to reduce the stress on the solder and thereby to reduce the damaging accrual of solder strain. Unfortunately, a second manifestation of lead stiffness is to prolong the application of stress during periods of loading dwell. If the dwell period is sufficiently long, the elastic stress in the flexible leads will fully relax through creep of the solder joint, and no strain reduction will be realized. The time required for significant stress relaxation to occur is largely controlled by the stiffness of the part-lead-board system, which sets the initial solder stress for a fixed load displacement and governs the rate at which the stress decreases as the solder strains. For loading conditions involving highly flexible leads, stress decreases slowly with increasing strain; this provides the conditions for the accrual of large solder strains over prolonged time periods.

Creep Strain during Stress Relaxation

Because creep strain development during stress relaxation is such an important part of solder joint performance with flexible leaded parts, it is useful to first carefully examine the dynamics of simple elastic stress relaxation before proceeding to more complex cyclic loading conditions. An understanding of stress relaxation is also germane to the issue of long-term creep rupture of solder-joint systems that have accumulated built-in residual stresses following the soldering operation. Such stress can occur due to differential expansion upon assembly cool-down following machine soldering, or due to elastic deflections applied to displace a misaligned lead during hand soldering.

Figure 3-1 presents a schematic representation of the elastic stress relaxation problem where the spring stiffness (K) is the effective stiffness of the combined solder-lead system; for the simple system shown in Fig. 3-1, this effective stiffness is given by:

$$K=(1/K_L + 1/K_S)^{-1} \qquad (9)$$

where

K_L = lead stiffness (lb/in)
K_S = solder stiffness = AE/L (lb/in)
L = solder length (in)
A = solder cross-sectional area (in^2)
E = modulus of elasticity of solder ($\approx 4 \times 10^6$ psi)

The stress relaxation problem is initiated by instantaneously elongating the outboard end of the spring by amount ΔX and then holding it at this position; this applies an initial stress ($\sigma_o = K \Delta x/A$) to the solder, where A is the cross-sectional area of the solder. As the solder creeps under the applied stress, the spring load gradually decreases and the creep rate slows.

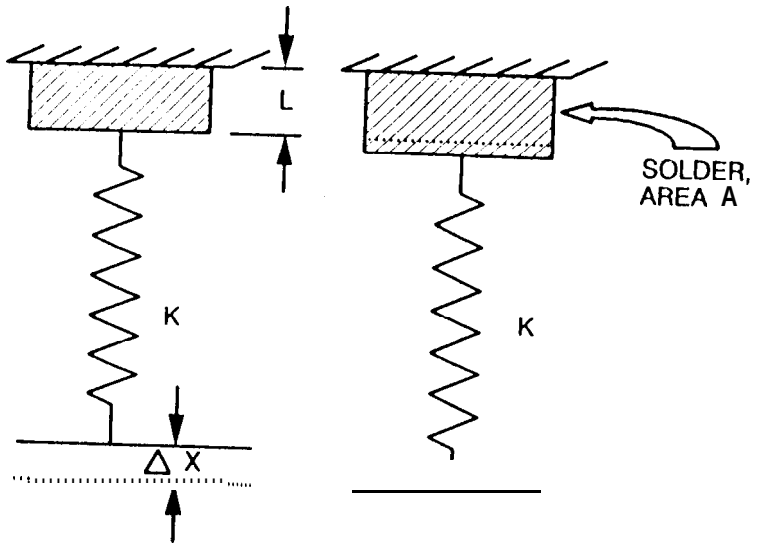

Fig. 3-I. Schematic of single-node solder element with series spring representing the combined elastic flexibility of the solder and electronic component lead,

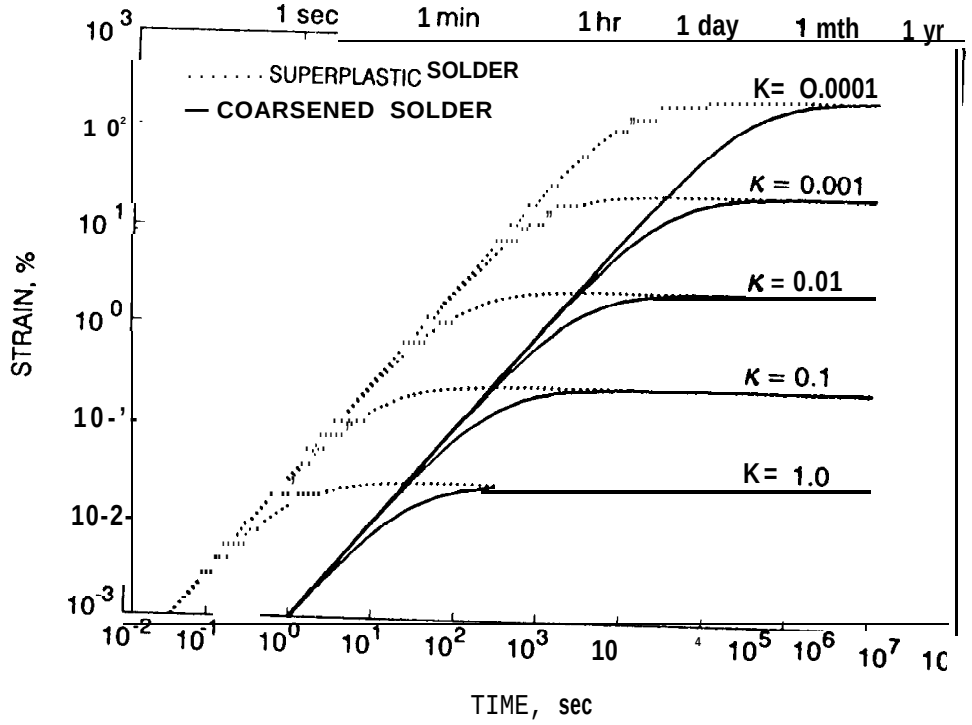

Fig. 3-2. Creep-relaxation response of solder as a function of relative spring stiffness (κ) for a fixed initial loading stress of 1 ksi

Eventually the solder creeps the total distance Δx, and the spring load and solder stress reduce to zero.

To obtain a quantitative feel for the stress relaxation behavior of solder, it is useful to examine two cases: one with a displacement ($\Delta x = \sigma_0 A/K$) corresponding to an initial solder stress of σ_0 = 1 ksi, and the second with a displacement ($\Delta x = L/10$) corresponding to a 10% solder strain upon complete stress relaxation. The 1 ksi initial-stress scenario represents typical conditions immediately following a large deflection that exceeds the solder yield strength; in this instance the solder starts with a stress close to the yield stress independent of lead stiffness, The second case represents a fixed lead offset that doesn't exceed the solder yield strength. Note that yield stress for our purposes is the stress in Figure 2-4 at which the strain rate leads to near instantaneous straining (e.g. $\dot{\epsilon} > 10^{-2}$ sec^{-1}).

Figures 3-2 and 3-3 present stress relaxation plots computed for these two cases using the authors' finite-element creep simulation computer program. The computations are based on the room-temperature solder constitutive properties of "superplastic" and "coarsened" solder as displayed in Figures 2-4 and 2-5. The results are presented parametrically as a function of spring stiffness ratio κ, where κ is the ratio of the stiffness of the combined solder-lead system (the spring in Fig. 3-1) to the stiffness of the solder element by itself, i.e.

$$\kappa = K/K_s = KL/AE \qquad (10)$$

Because K is the effective stiffness of the combined solder-lead system as defined by Equation 9, κ = 1 corresponds to solder with no additional lead flexibility, and κ =0.1 and 0.01 represent systems 10 and 100 times more flexible than the solder itself, respectively.

From Figure 3-2 it can be seen that without the addition of system flexibility the maximum stress-relaxation strain that can occur in solder-by itself is a negligible 0.025%. This strain equals the initial elastic strain ($\epsilon = \sigma_0/E$) in the solder at 1 ksi, and is seen from Figure 2-1 to correspond to a fatigue life of tens of, millions of cycles. This is important because it confirms that creep and stress relaxation are not important unless significant additional system flexibility is present.

In contrast, notice that for the same initial 1-ksi solder stress, flexible leads can result in very damaging levels of stress-relaxation strains. Making the leads more flexible clearly worsens the problem when the loading condition is a modestly-high fixed initial stress. This is apparent by noting that the final creep strain (ϵ_f) is defined by:

$$\epsilon_f = \Delta x/L = \sigma_0 A / K L = \sigma_0 / \kappa E \qquad (11)$$

To prevent stress-relaxation strain from nulling the effectiveness of flexible strain relief elements over multi-hour loading cycles, it is necessary to limit the maximum creep strain rate to well below 10^{-6} sec^{-1}; this corresponds to approximately a 1% strain over a 3-hour period. From Figure 2-4 it can be

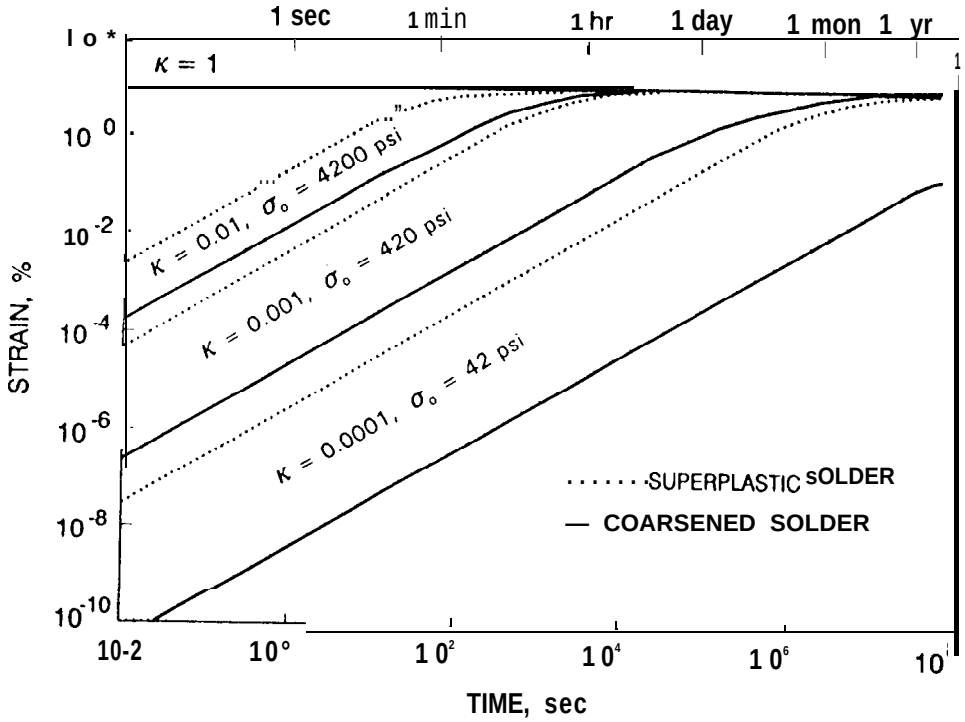

Fig. 3-3. Creep-relaxation response of solder as a function of relative spring stiffness (κ) for a fixed spring-tip displacement (Δx) corresponding to a 10% strain upon complete stress relaxation,

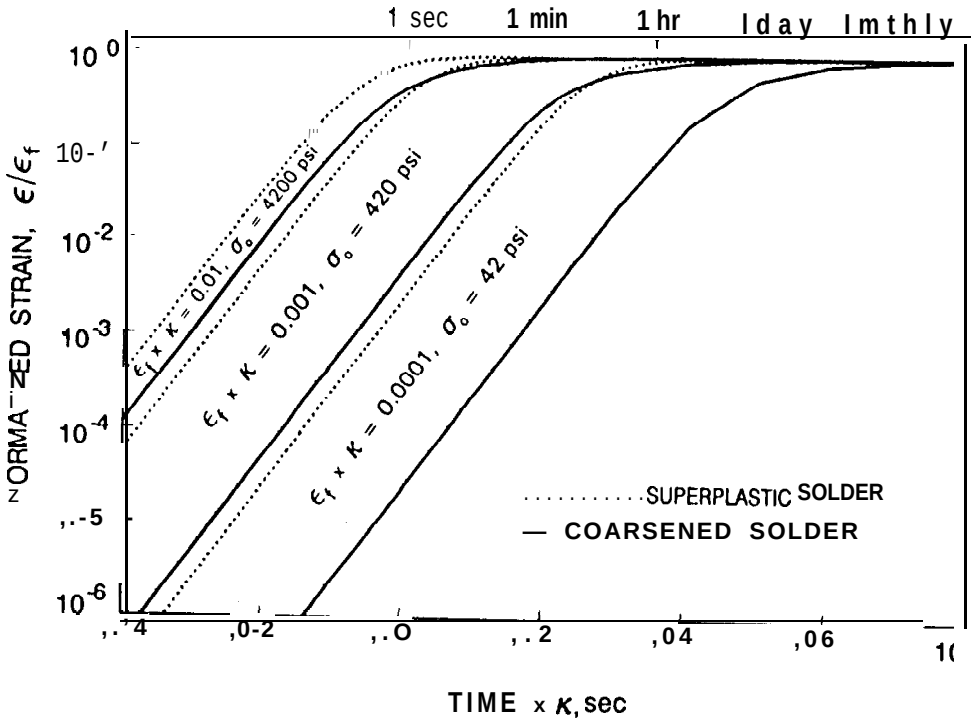

Fig. 3-4. Creep-relaxation Master Curves that describe creep-relaxation response of solder as a function of relative spring stiffness (K) for initial stress (σ_0) or a spring-tip displacement (Ax) corresponding to a final strain (ϵ_f) upon complete stress relaxation.

seen that this requires that the maximum solder stress be less than 100 psi at room temperature--a small fraction of the solder yield stress.

This requirement for low initial stress ($\sigma_0 < 100$ psi) is also apparent from the case of a fixed initial lead deflection as shown in Figure 3-3. Because Equation 11 defines a fixed relationship between initial stress (σ_0), strain displacement (ϵ_f), and lead stiffness (κ), Figure 3-3 is marked with the initial stress corresponding to each of the κ values. In this case only leads with a relative stiffness (κ) less than around 0.001 have low initial stress and limit stress relaxation during a typical multi-hour loading cycle, Notice also the important difference made by the solder metallurgical properties ("superplastic" versus "coarsened" as defined in Figure 2-4).

By noting the similarity between Figures 3-2 and 3-3, it may be suspected that a single relationship can be used to describe both; indeed this is true, and Figure 3-4 provides this relationship as a so-called Master Curve for creep relaxation. With it, the creep relaxation behavior with any initial stress or spring-tip displacement can be easily determined.

Strain Range during Isothermal Mechanical Cycling

As the next step in systematically understanding the role of lead flexibility on solder joint life, it is useful to extend the single-node solder model presented in Figure 3-1 by imposing a cyclic mechanical displacement to the end of the spring instead of the fixed-displacement used in the stress-relaxation computations. Figures 3-5 and 3-6 describe the influence of lead stiffness, cyclic frequency, and solder temperature on the computed strain response to the cyclic displacement profile noted in Figure 3-7. Because the amplitude of the profile was chosen to correspond to a maximum solder strain of 42% during circumstances of complete stress relaxation, each of the curves in Figures 3-5 and 3-6 approaches this 42% strain value asymptotically.

Looking first at Figure 3-5, it can be seen that very flexible leads with $\kappa < 0.001$ significantly reduce the generated strain range from cyclic loading. In addition, for. highly flexible leads, the strain range amplitude is inversely proportional to frequency--thus proportional to dwell time; this is expected for constant applied stress (minimal stress relaxation), which causes constant creep strain rate during each half cycle. For very low frequencies, or very stiff leads, the solder creeps to its asymptotic equilibrium value; under such conditions solder strain is determined by the lead deflection and is independent of frequency.

Turning next to solder temperature effects, Figure 3-6, which is similar to Figure 3-5, provides the computed response of cyclic loading to solder temperature. The results for highly flexible leads are again predictable, and reflect a factor of 1.5 to 2.0 increase in strain range for each 10°C increase in temperature. This is in agreement with the classical creep rate dependence on temperature [26] shown in Figure 2-5.

Lastly, Figure 3-8 describes the effect of variable loading displacement (Δx as defined in Fig. 3-7) on solder strain range; in this case the solder temperature is held fixed at 25°C and cyclic frequency is held at 1 cycle per

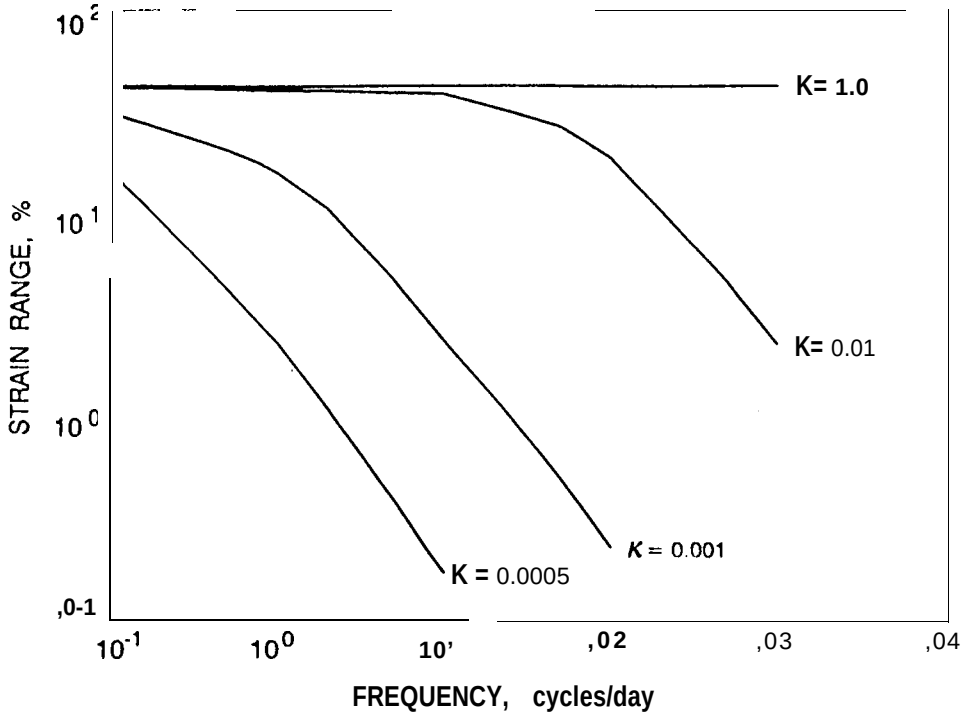

Fig. 3-5. Effect of eye" ic frequency of loading and relative spring stiffness (κ) on computed solder strain range,

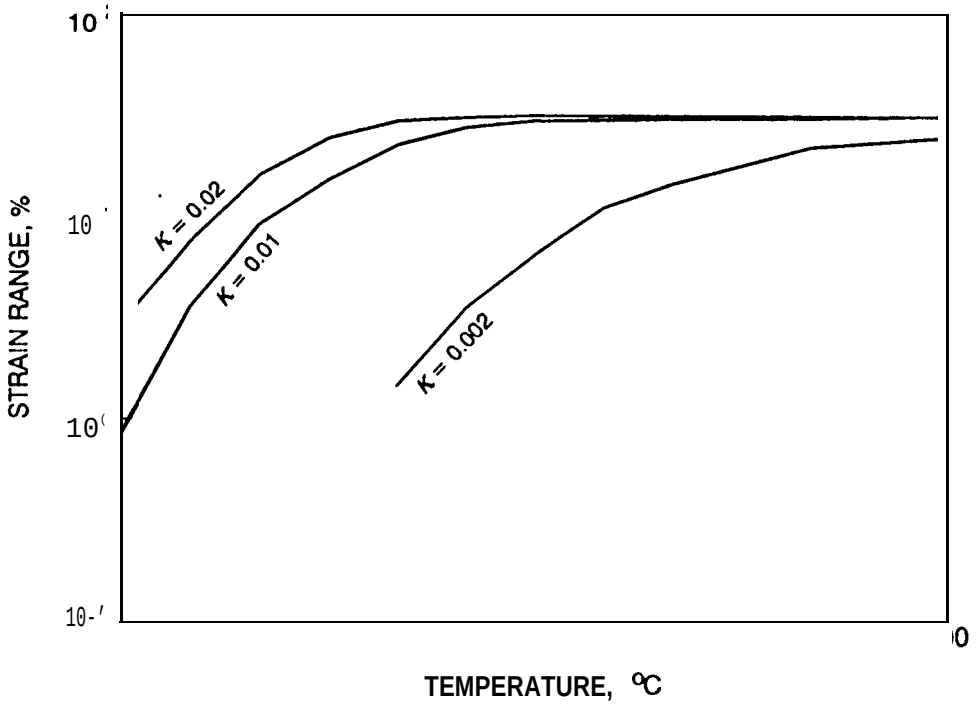

Fig, 3-6, Effect of solder temperature and relative spring stiffness (κ) on computed solder strain range.

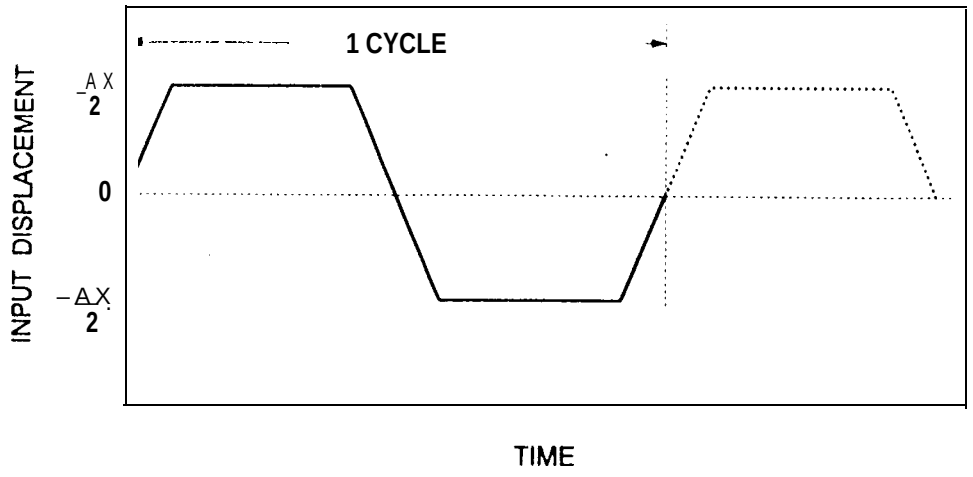

Fig. 3-7, Cyclic displacement profile (Δx versus time) used for isothermal strain studies with single-node spring-loaded solder element.

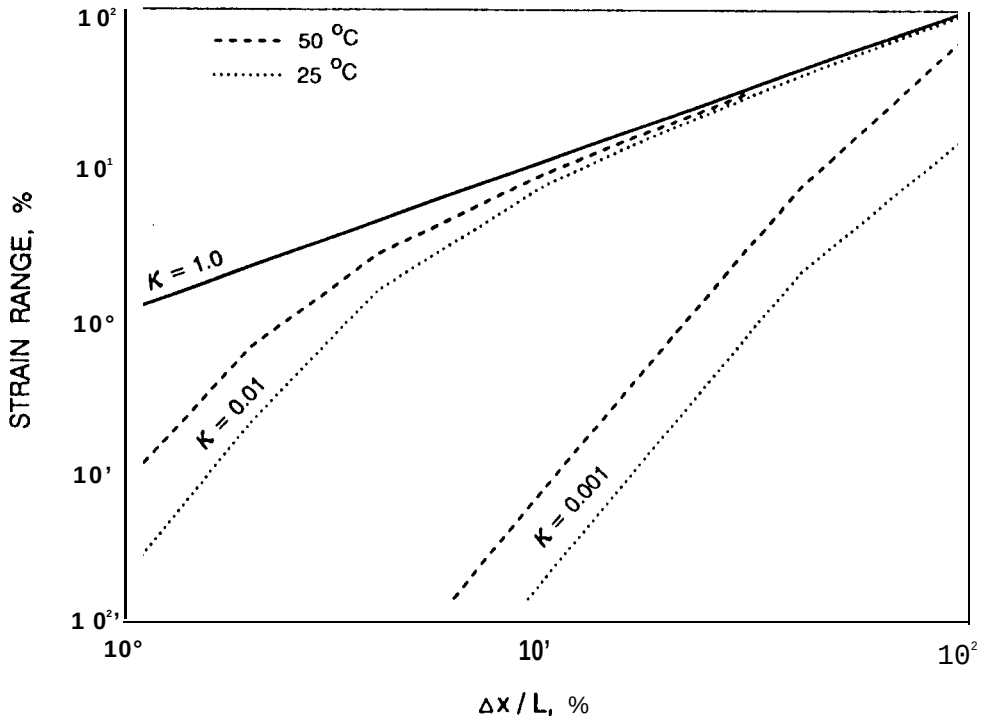

Fig. 3-8. Effect of input displacement amplitude (Δx) and relative spring stiffness (κ) on solder cyclic strain range (Δε).

3 hours. Note that for highly flexible leads the strain range varies approximately as the square of the deflection range (Ax), and for very stiff leads the curves asymptotically approach the linear ($\Delta\epsilon$ = Ax/L) dependency defined by an infinitely stiff lead (i.e. κ = 1). Also note that for a fixed Ax, the strain range for highly flexible leads varies approximately as the square of the relative spring stiffness (κ).

This stiffness and deflection-range dependence for highly flexible leads follows directly from the constitutive properties of solder as presented earlier in Equation 8. For the case of minimal stress relaxation (i.e., constant stress during each loading half cycle), the strain rate $\dot{\epsilon}$ is approximately constant; thus the total strain range for each cycle is

$$\Delta\epsilon = 2 \int \dot{\epsilon}\, dt = 2\, \dot{\epsilon}\, \tau \qquad (12)$$

where (τ) is the half-cycle dwell time. Combining Equation 12 with the constitutive properties defined by Equation 8 gives

$$\Delta\epsilon \propto \tau\, \sigma^{n}\, g^{-p}\, \xi^{(T/10)} \qquad (13)$$

where

σ = solder stress
n = creep exponent (typically n = 2 to 3)
g = grain size
p = grain size exponent (typically p = 1.6 to 2.3)
ξ = temperature dependence per 10°C (typically ξ = 1.5 to 2)
T = solder temperature (°C)
τ = half-cycle dwell time

Noting that the solder stress is determined by σ = K Ax/A gives

$$\Delta\epsilon \propto \frac{\tau\, K^{n}\, AX^{n}}{A^{n}\, g^{p}}\, \xi^{(T/10)} \qquad (14)$$

where (A) is the cross-sectional area of the solder under load. This expression for very flexible leads notes that the strain range is proportional to roughly the square of the lead stiffness, the square of the lead displacement, and the inverse square of the grain size as defined by the values of n and p associated with Figure 2-4 and Equation 8. This agrees with, and provides physical insight into the numerical simulation results presented in Figure 3-8, For the limiting case of an infinitely rigid lead with no creep, Equation 14 reduces to $\Delta\epsilon \propto \Delta X$.

The important implication of Equation 14 is that, for very flexible leads, the dependency of the strain range on operational parameters is fundamentally determined by the constitutive properties of solder. If these constitutive properties change for different solder types or aging conditions, then the power-law dependencies will also change.

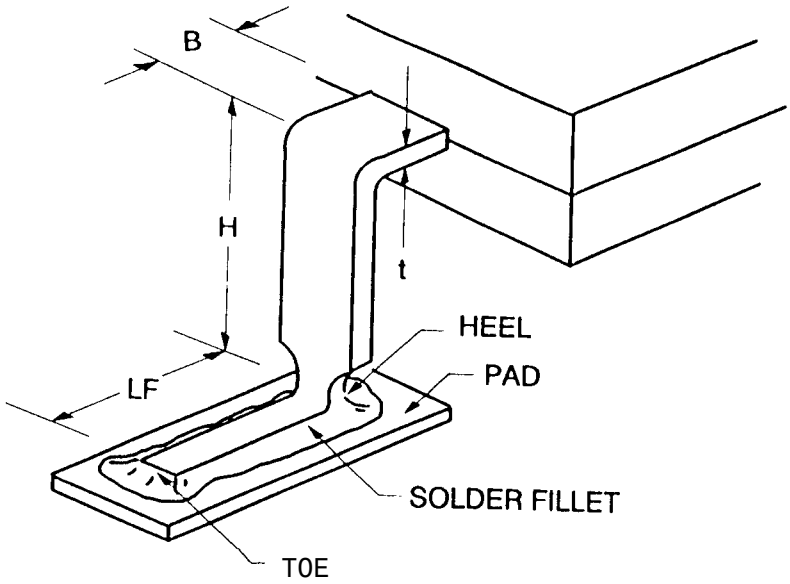

Fig. 3-9. Solder-joint nomenclature and dimension definitions for flat-pak parts mounted with gull-wing leads.

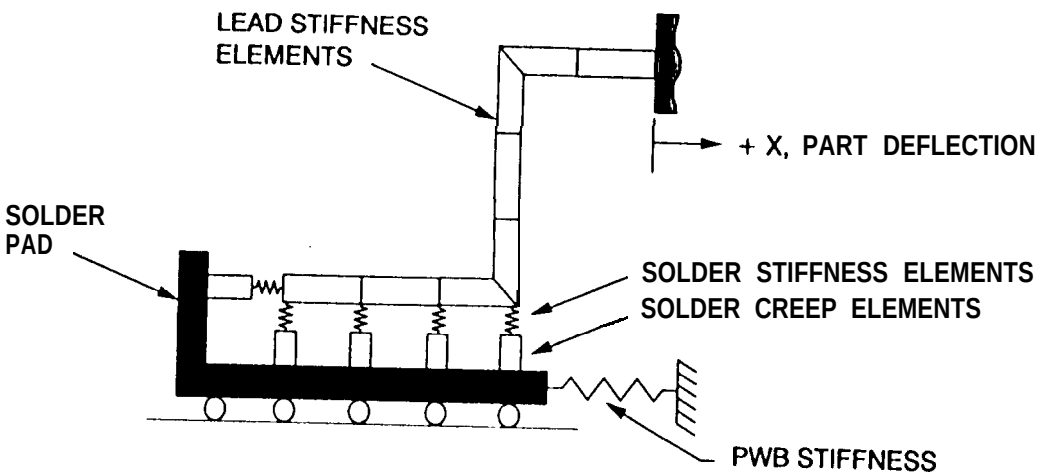

Fig. 3-10. Schematic of finite element elastic-plastic-creep model of solder joint with gull-wing lead.

Complex Strain Behavior with Leaded Parts

The preceding discussion has highlighted the important parameters influencing the development of creep strain in elastically loaded solder joints. Because creep rate is strongly dependent on the applied stress, flexible leads that lower the stress can greatly diminish the developed strain. However, with flexible leaded parts, such as a gull-wing flat-pak shown in Figure 3-9, the solder is subjected to a much more complex loading environment than the previously discussed single node model. There are three principal contributors to this increased complexity:

1) The solder joint is spatially distributed and attached to the part lead at multiple locations. For clarity, it is often useful to consider the joint as made up of numerous independent solder elements attached in parallel between the part lead and the substrate.

2) The complex lead geometry causes the individual solder elements to be loaded by different stress levels in different directions. This causes some solder elements to be primarily loaded normal to the board in tension-compression, while others are primarily loaded parallel to the board in shear. The lead itself undergoes complex motion containing rotation as well as translation.

3) Because the lead is flexible, the load on the individual solder elements is highly interactive and often timewise out of phase. For example, on a gull-wing lead, the solder attaching the toe of the lead cannot be significantly loaded until the heel has deflected. This causes a phase shift between when the heel and toe undergo maximum straining. This lack of simultaneity is important because it implies that there is no single point in time when each element of the solder is at its maximum strain level; thus no single snap-shot in time can be used to evaluate the strain range ongoing in different elements of the solder joint.

One of the only practical means of analyzing solder joints with flexible leads is the non-linear finite element creep simulation approach discussed earlier, Figure 3-12 illustrates the solder strain response computed for a flat-pak part using the model shown in Figure 3-10 and the lead-tip displacement profile shown in Figure 3-11; this tip deflection (± 0.0003 inches) is the same magnitude as would be seen by a ceramic chip mounted to an FR-4 board and cycled between -32 and +100°C.

The results presented in Figure 3-12 correspond to a gull-wing lead with a 20-mil height, a constant 32.5°C operating temperature, and a three-hour loading cycle. The structure of the finite-element model implicitly accounts for the important geometry and distributed flexibility of the lead, and the distributed nature of the solder joint.

In the results shown in Figure 3-12, the heel and toe rock up and down applying normal-to-the-board tension and compression to the solder. Note that the heel and toe strains are almost 90 degrees out of phase with respect to one another, and are substantially different in amplitude. Although some asymmetry occurs at the start of loading, the strain eventually becomes

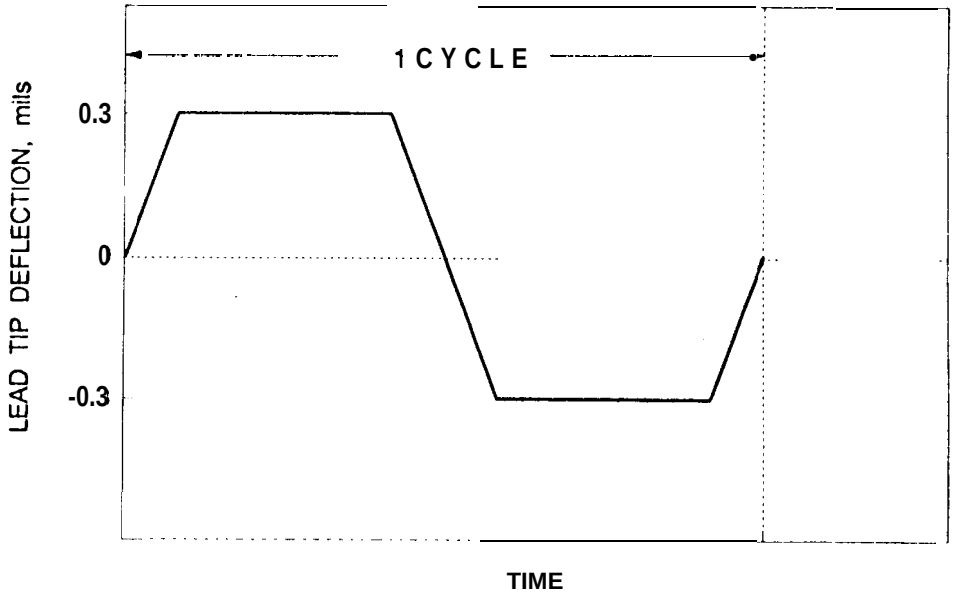

Fig. 3-11. Cyclic displacement profile (Δx versus time) used for isothermal strain response studies with gull-wing flat-pak.

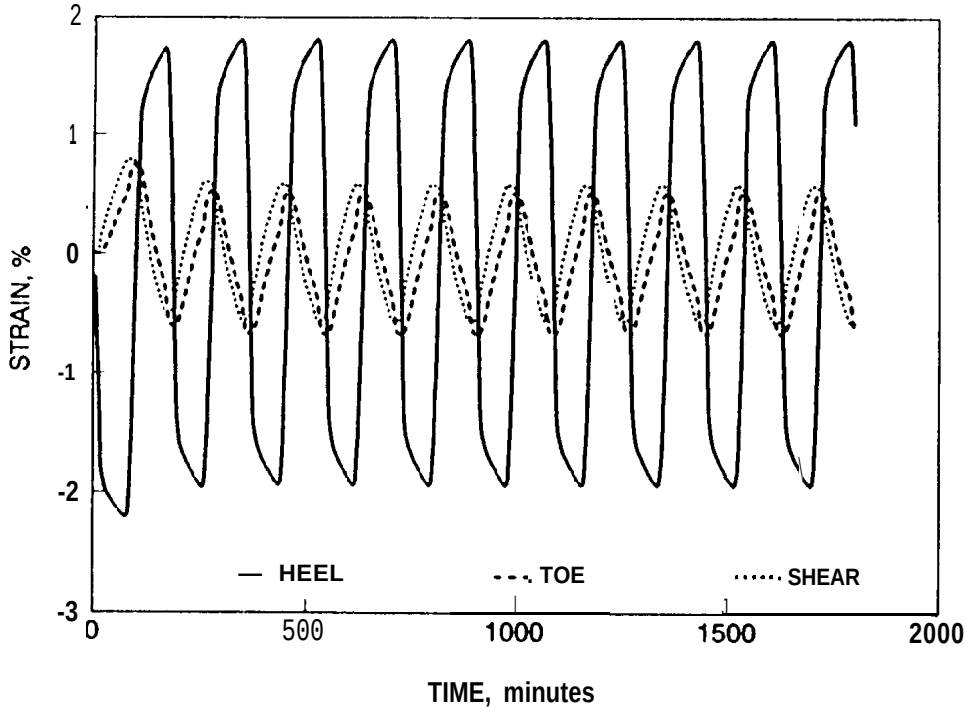

Fig. 3-12. Typical heel, toe and shear strain response of mechanically cycled gull-wing lead (20-mil high flat-pak).

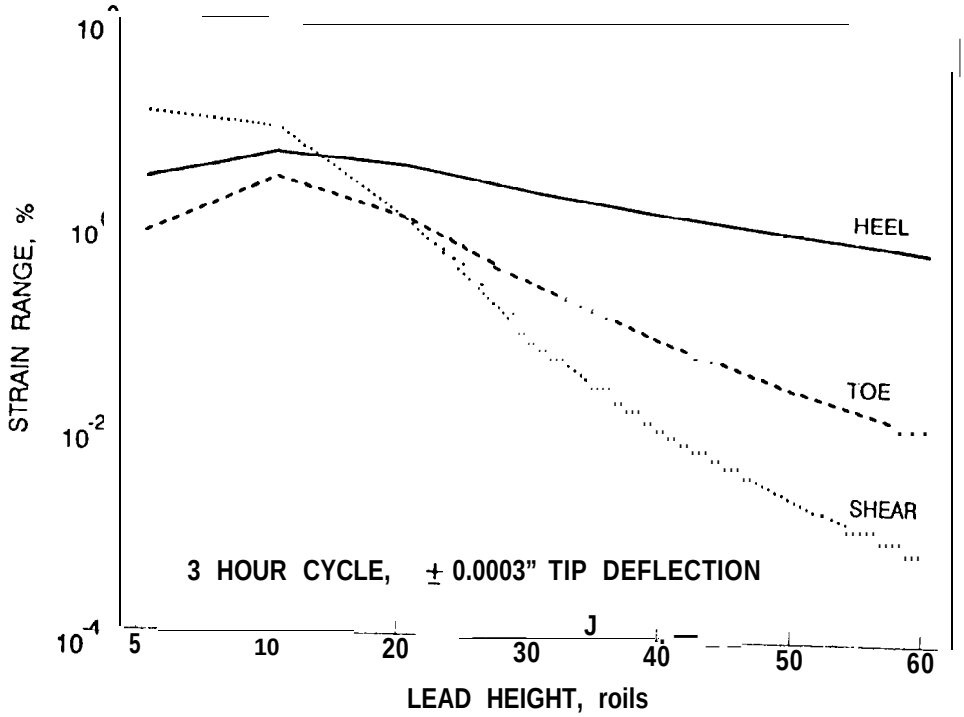

Fig, 3-13. Computed dependence of strain range on lead height for flat-pak parts with gull-wing leads.

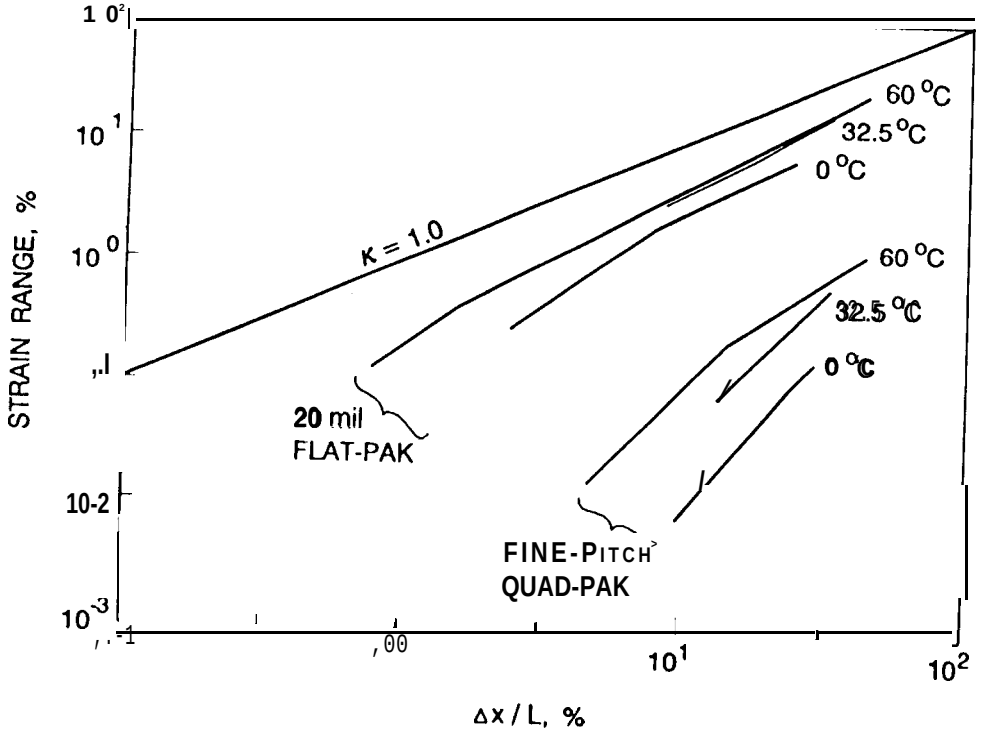

Fig. 3-14, Dependence of solder strain range on lead deflection range (Δx) and temperature for gull-wing leads with different stiffnesses.

symmetrical about the zero-strain axis.

Figure 3-13 expands on the results of Figure 3-12 by describing the dependence of the gull-wing solder strain range on lead height, for the same 3-hour cycle and tip-deflection profile shown in Figure 3-11. Notice that horizontal shear strain, which is negligible with the taller lead heights, becomes dominant when the lead height is reduced below 20 roils. Notice also that the strain at the toe decreases much more rapidly with increasing lead flexibility than does the strain at the heel. These results graphically illustrate the complex inter-dependency between shear strain and heel-toe tension-compression strain with gull-wing or J-lead type leads. This interdependency reflects the fact that the effective stiffness ratio (κ_s) in the horizontal shear direction drops off much faster with increasing--lead height than does the effective stiffness ratio (κ_t) in the normal-to-the-board tension-compression direction, Table 3-1 presents lead dimensions and approximate κ values for the popular component lead types illustrated earlier in Figure 1-1. Nomenclature are presented in Figure 3-9

Because of these complex lead stiffness interdependencies, it is instructive to revisit the sensitivity of strain range to lead deflection range Ax, solder temperature, and cyclic frequency noted in the last section for a single node solder joint. Figure 3-14 combines the effects of solder temperature, lead stiffness and lead deflection range into a single plot. Notice that the 20-mil flat-pak lead is quite stiff in that it exhibits little strain range reduction, near linear strain dependency on Ax, and very little temperature dependency. This is indicative of near complete creep relaxation. In contrast, the Quad-pak with much more flexible fine-pitch leads (see Table l-l) significantly reduces the strain range; as a consequence, it exhibits the strong (Δx^n) strain dependency and Arrhenius temperature dependency associated with the creep properties of solder in Figure 2-4 and 2-5 and Equation 14. Figure 3-15 amplifies on the temperature dependency of strain range for these two lead configurations and graphically illustrates that parallel-to-the-board shear strain has a much stronger temperature dependency than does the normal-to-the-board tension-compression strain at the lead's heel. This is caused by the relative differences in κ for the shear and tension-compression loading directions, and by the complex interplay associated with' simultaneous straining in these two orthogonal directions. This complex strain interdependency will become even more important in the thermal-cycling environments discussed in the next section.

Lastly, Figure 3-16 displays the computed dependence of strain range on loading frequency for gull-wing leads with a constant ± 0.0003" lead deflection amplitude, as shown in Figure 3-11, and 32.5°C solder temperature, Notice that the frequency dependence of the more highly flexible fine-pitch quad-pak lead is very similar to the l/frequency dependence previously noted in Figure 3-5 and Equation 14. In contrast, the 20-mil flat-pak lead is seen to exhibit a significantly lower frequency dependence consistent with its higher stiffness.

Table 3-1. Approximate dimensions and relative stiffnesses for popular electronic component leads,

	Typical Flatpack	Gullwing Dip	Gullwing Quad	J Lead Quad
LF, roils	50	50	40	45
H, roils	20	115	100	115
B, roils	35	20	17	30
t, roils	7	11	6.5	9
EI_{LF}, lbmil^2	8500	34000	3910	19550
EI_{H}, lbmil^2	8500	113050	3910	29750
EI_{B}, lbmil^2	8500	113050	3910	20400
κ_t, Heel	0.009	0.0015	0.00008	0,0004
κ_s, Shear	0.003	0.0005	0.00003	0.0001

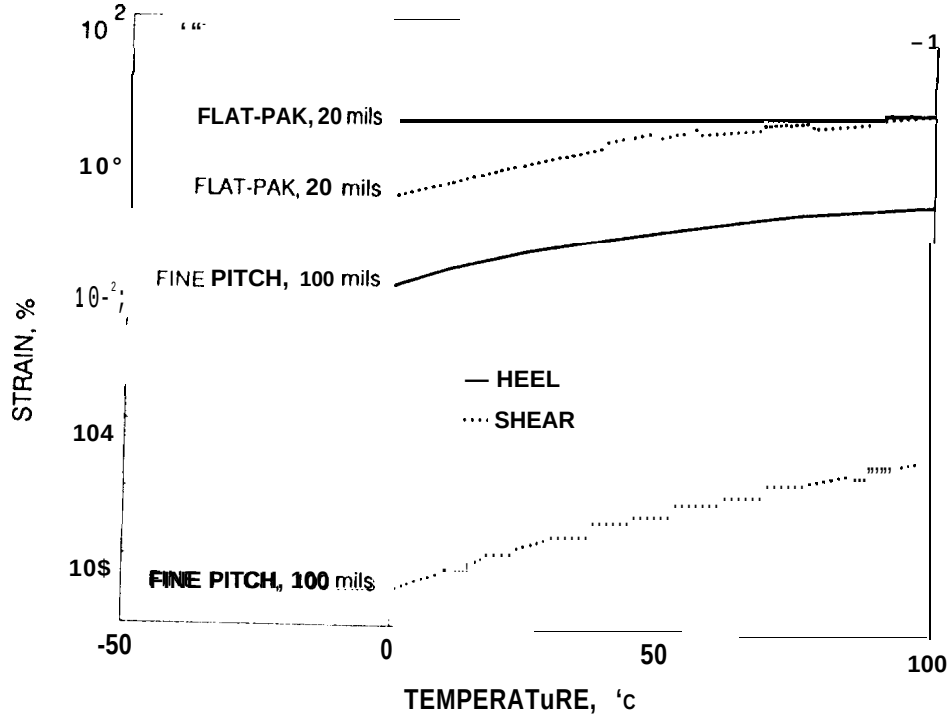

Fig. 3-15. Temperature dependence of solder strain range components for gull-wing leads of different stiff nesses.

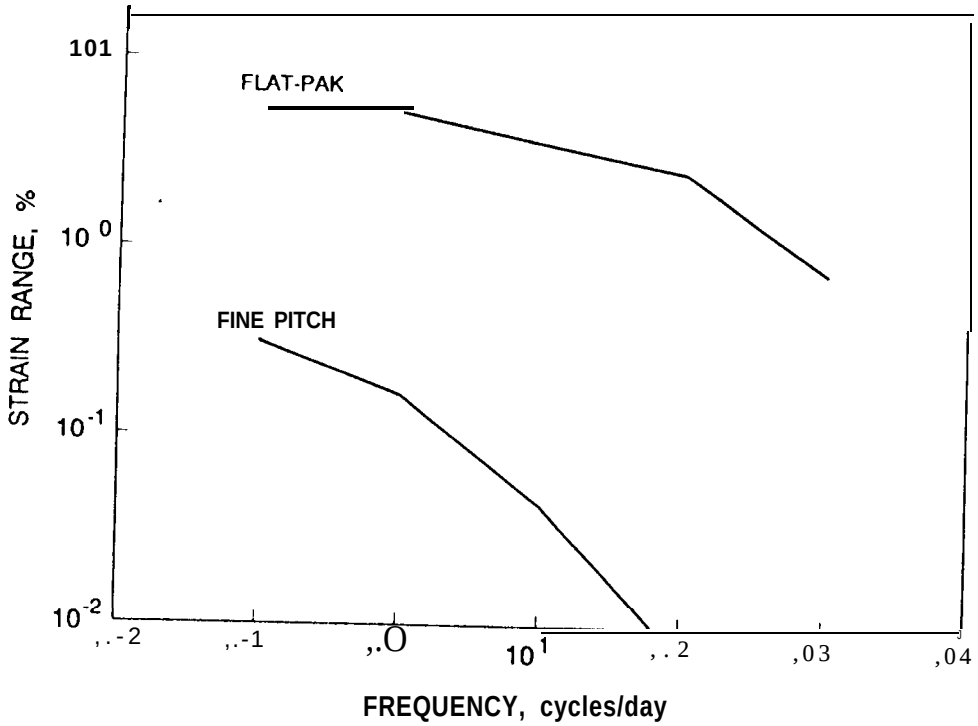

Fig, 3-16. Dependence of solder strain range on cyclic frequency for gull-wing leads of different stiffnesses.

IV. ROLE OF LEAD STIFFNESS WITH THERMAL CYCLING

Thermal cycling, or thermal-mechanical loading as it is often referred to, generates similar displacement loading profiles to those noted in the last section, However, the displacements generally arise from differential thermal expansions and contractions of the electronic part relative to those of the substrate to which it is mounted. Although the resultant lead deflection may be similar, a fundamental difference between isothermal mechanical cycling and thermal cycling is the fact that the solder is at different temperatures at different points in the loading cycle. This alters the creep strain contributions from various parts of the cycle, and introduces important asymmetries in the resulting strains. With shallow cycle depths the differences between isothermal cycling and mechanical cycling can be quite small and accurately ignored. However, with increasing depth, the difference can become very pronounced and must be carefully considered.

Figure 4-1 displays the computed strain response during a representative field-application thermal cycle with 15°C temperature range (25°C to 40°C) and 3-hour cyclic period. The input horizontal displacement (Δx) corresponds to the thermal mismatch between a ceramic flat-pak (x = 1.23 cm, α_a = 6 ppm/°C) and an FR-4 PWB bonded to an aluminum substrate (α_b = 20 ppm/°C). The mean temperature is 32.5°C in this case, and the displacement variation, shown at the bottom of Figure 4-1, corresponds to a ±7.5°C temperature swing over the 3-hour cycle. The first two cycles of computed strain variation at the solder joint heel and toe are shown in the top of Figure 4-1 for a typical 20-mil lead height and 7-roil lead thickness. The maximum strain range (about 0.17%) occurs as a normal-to-the-board tension-compression at the heel, while the toe undergoes much less strain.

Creep Ratcheting

Perhaps the most important difference between isothermal mechanical cycling and thermal cycling is the existence of progressive strain drift or "creep ratcheting" that accompanies the alternating fatigue component in long-term thermal cycling. As an example, Fig. 4-2 displays the long-term strain-cycling behavior of the flat-pak part used in Fig. 4-1, together with the long-term behavior of parts with both taller (30-mil) and shorter (10-mil) lead heights, Although the computed cyclic strain ranges (0.62% and 0.051%, respectively) vary as expected with the increasing lead height, the solder also undergoes a lead-height-dependent long-term strain drift. In this example, this progressive strain drift is 2.5%, 0.5%, and 0.04%, respectively, after 1000 thermal cycles.

This long-term drift is referred to as "creep ratcheting" in recognition of its ratchet-like directional dependence, which stems from the strong temperature dependence of creep during different phases of the loading cycle. This creep-ratcheting phenomenon has only recently been understood through the use of finite element strain simulation analyses [1,2,19].

To further illustrate the observed creep ratcheting phenomenon, a pair of

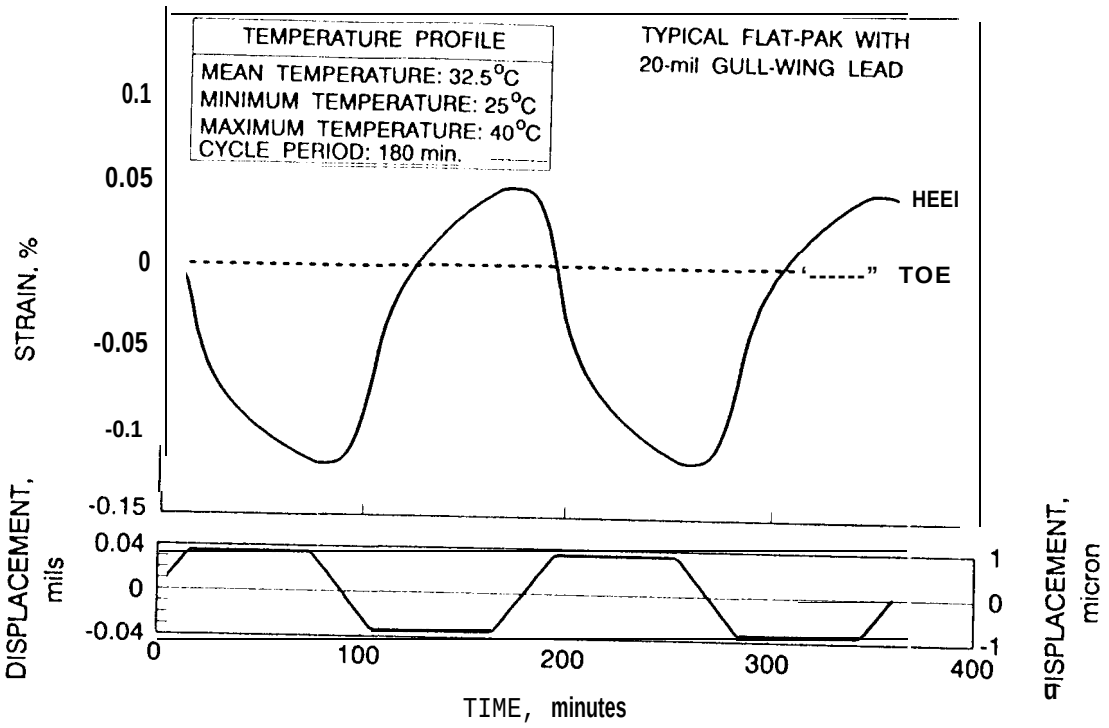

Fig, 4-1. Example flat-pak lead displacement and solder strain response to 15°C thermal cycle with 3-hr period.

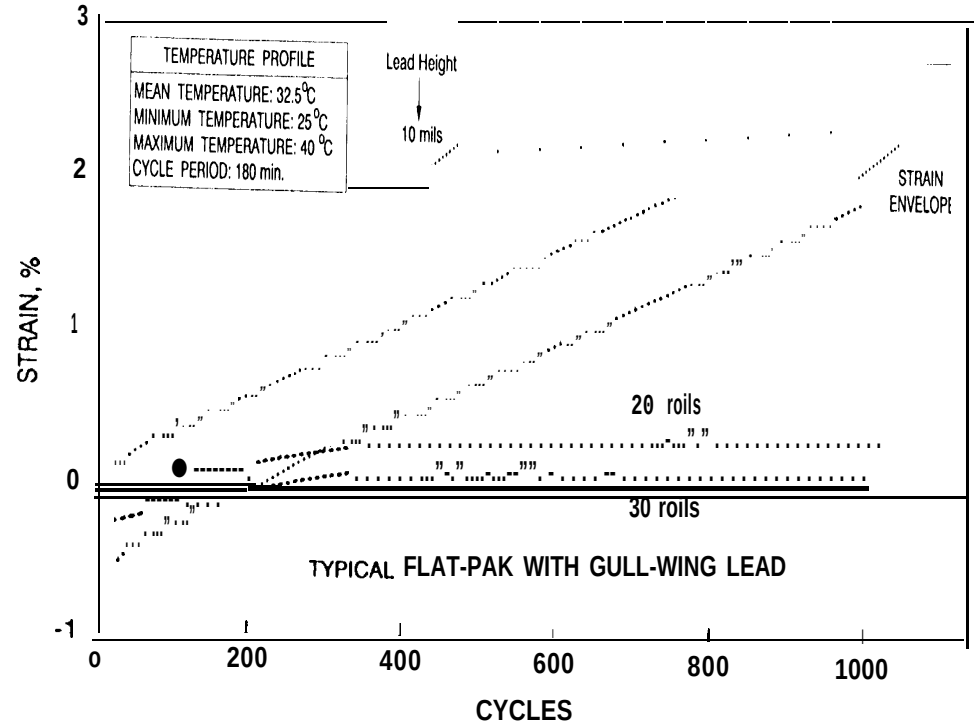

Fig. 4-2. Thermal cycle strain response showing dependence of creep ratcheting on lead height.

simulations is presented in Figure 4-3, based on the same 20-mil flat-pak used in Figure 4-1, but with the displacements provided in one case by the 25°C to 40°C thermal cycle, and in the other case by an isothermal mechanical cycle with the same lead displacement and 32.5°C mean temperature. The left side of the figure compares the strain variations in the first five cycles, It can be seen that the shapes and amplitudes of the two cases are very similar. However, after 1000 cycles, the mechanically cycled straining remains essentially unchanged and is symmetrical about the neutral position. The thermally-cycled straining, on the other hand, has ratcheted--in essence, drifted-- an additional 0.6% over and above the mechanical cycling component,

The mechanics of creep-ratcheting can be better understood by studying the exaggerated movements occurring in deep temperature cycles (-35°C to 100°C); these are typical of qualification test levels for electronic circuit boards [29].

Figure 4-4 displays the tension-compression strain variations occurring between the 90th and 100th deep thermal cycle (range = 135°C, mean temperature = 32.5°C) as computed at the heel and at the toe for the same lead-solder system used in Figure 4-2. The rate of creep ratcheting is considerably larger for the 135°C cycle depth than for the 15°C cycle depth; this can be seen by comparing the data of Figures 4-2 and 4-4. Note that the tension-compression strains at the heel and toe are out of phase and that the toe strains have a very different time response than during isothermal cycling (Figure 3-10), The nature of the heel-to-toe rocking during thermal cycling causes the creep-ratcheting which causes a bias "drift" in a direction normal to the board -- away from the board if $\alpha_b > \alpha_p$, toward the board if $\alpha_b < \alpha_p$; recall that α_p and α_b are the CTES of the part and board, respectively.

To explore the fundamentals underlying the creep-ratcheting phenomenon, it is useful to examine closely the 135°C thermal-cycling simulation results. Figure 4-5 shows the computed shear stress variations for this thermal cycle (for $\alpha_b > \alpha_p$) overlaid on the corresponding data for isothermal mechanical cycling, i.e., with identical part displacement profiles. It is helpful to first examine the mechanics of the mechanical cycling, and then to contrast them with the observed differences for thermal-cycling.

Strain Development During Isothermal Mechanical Cycling

During the expansion phase of the isothermal mechanical cycle, there is a positive displacement of the part lead in the +x direction (defined in Figure 3-10), and a resulting horizontal force applied to the solder fillet in the +x direction. This force generates both horizontal shear stresses and vertical tension-compression stresses within the solder. The corresponding shear stress in the solder increases to a maximum as the displacement proceeds from point "a" to point "b" (Figure 4-5). During the dwell time ("b" to "c"), the stress relaxes due to creep until the displacement direction reverses ("c" to "d") and ultimately achieves a maximum displacement in the -x direction (point "e") just before the stress again undergoes creep relaxation during the dwell period. In essence, once a steady state condition is achieved, the shear stress variation during isothermal mechanical cycling is symmetrical relative

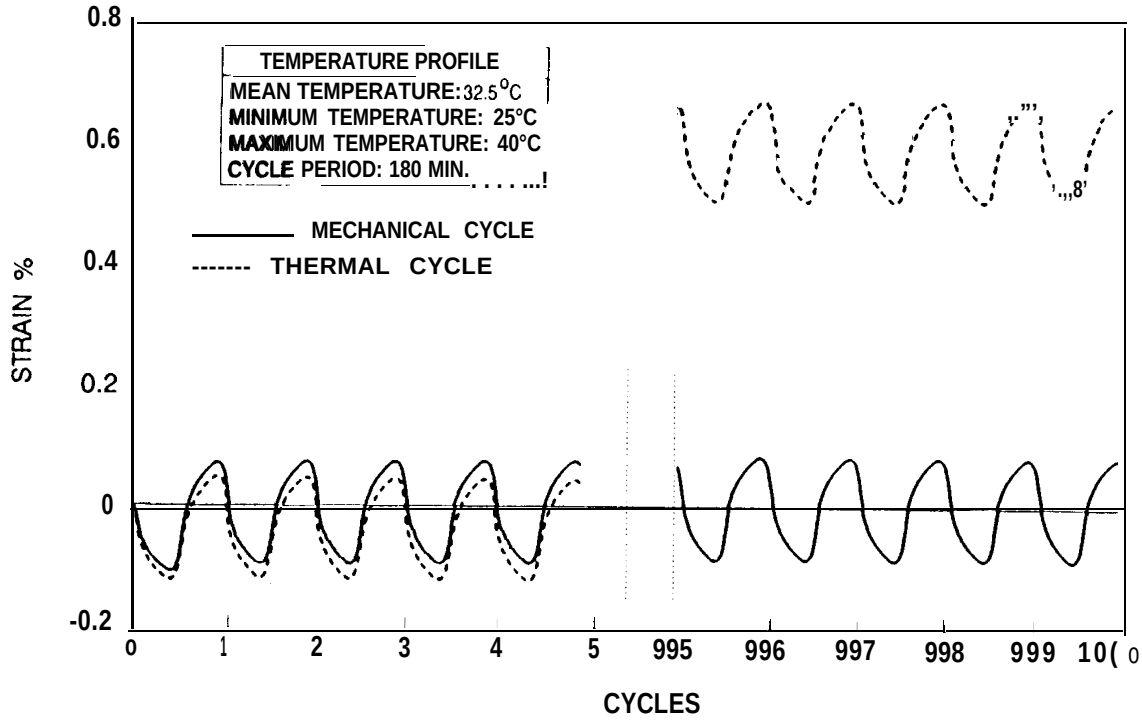

Fig. 4-3. Creep ratchet visible in thermal cycle strain response as compared with isothermal mechanical cycling.

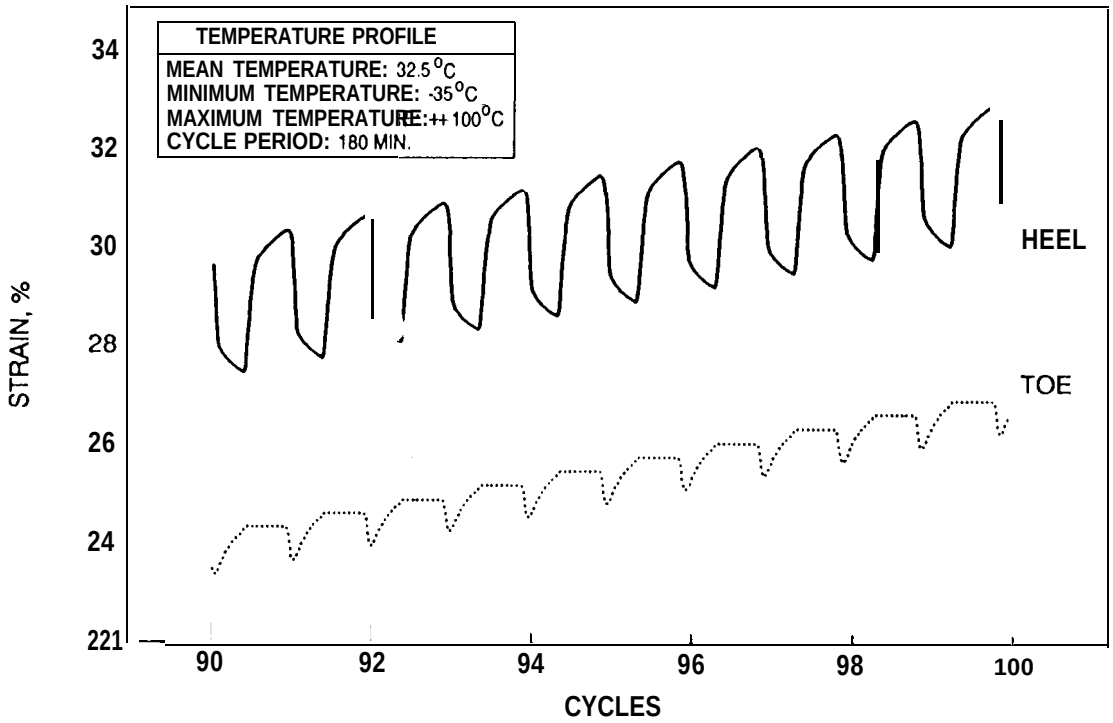

Fig. 4-4. Creep ratcheting apparent in heel and toe strain response to 135°C thermal cycling.

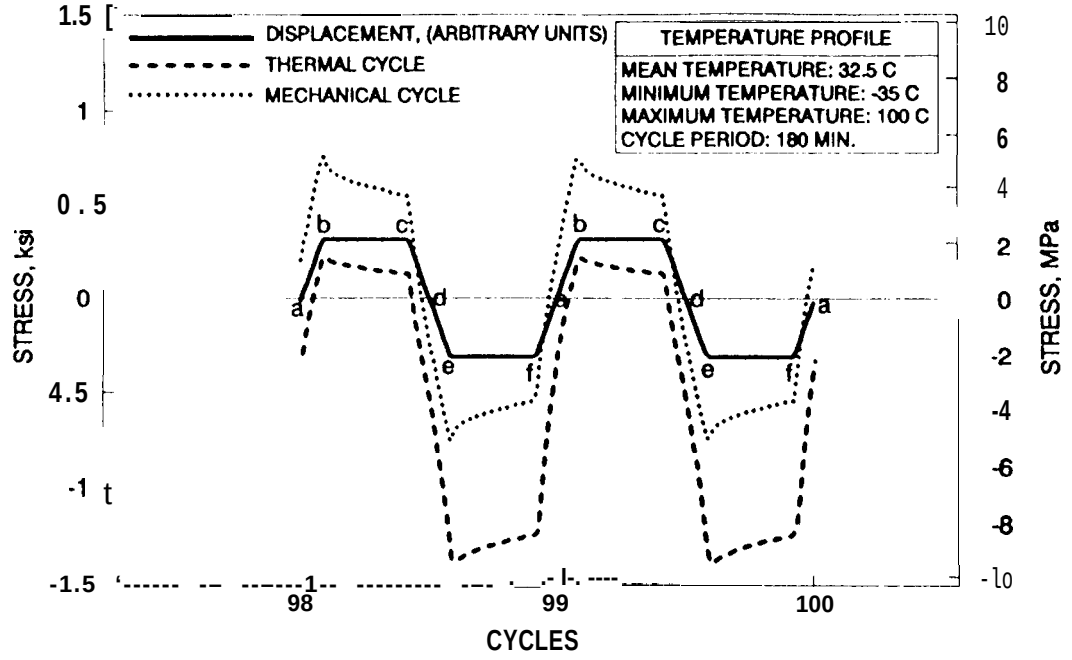

Fig. 4-5. Comparison of steady state shear stress vs. time for isothermal mechanical cycling and thermal cycling having the identical (shown) displacement.

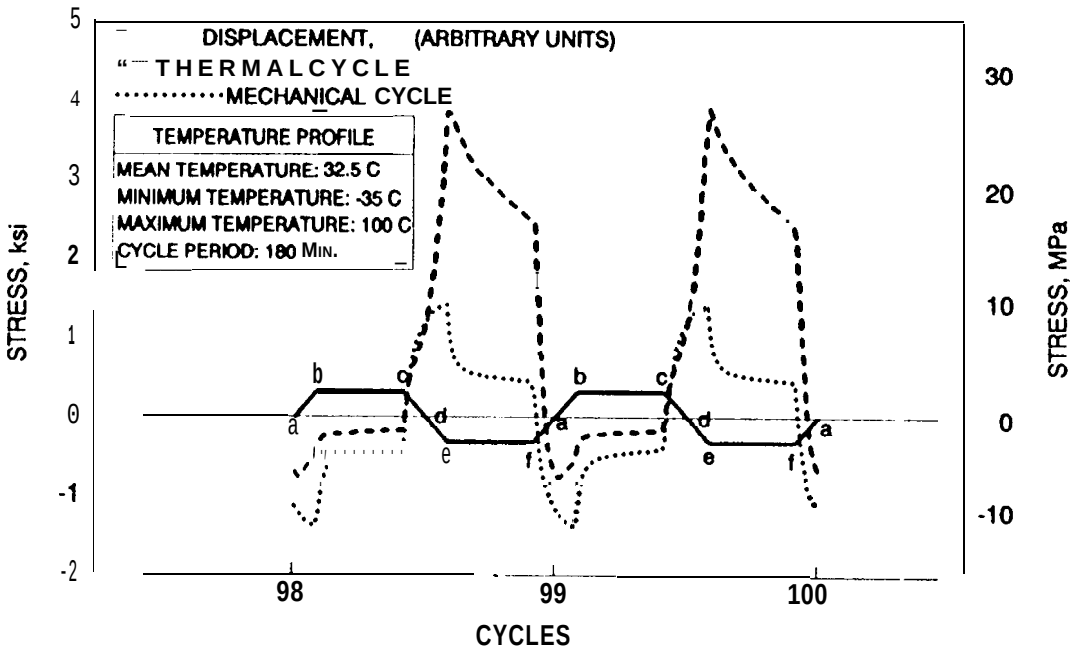

Fig. 4-6. Comparison of steady state heel stress vs. time for isothermal mechanical cycling and thermal cycling having the identical (shown) displacement.

to the neutral position and it closely tracks the displacement profile.

The corresponding tension-compression heel stress variation in isothermal mechanical cycling is also symmetrical about the zero strain axis, as shown in Figure 4-6. The heel is under compression, while the toe is under tension when the part displacement is positive. These stresses relax during the dwell time and reverse their sense when the part displacement changes direction.

Strain Development During Thermal Cycling

If the part displacements arise from differential thermal expansion-contraction during temperature cycling, the dynamics are quite different from those for isothermal mechanical cycling; this is because solder creeps much more rapidly during the higher-temperature portion of the cycle than during the lower-temperature portion, in accordance with Figure 2-5. The difference between isothermal mechanical cycling and temperature cycling manifests in the very first cycle. If the thermal cycle starts with cooling, a net initial displacement in the -x direction, the solder is quite creep-resistant because of the low temperature; the resulting shear strain is therefore very limited and most of the would-be solder displacement is absorbed by lead deflection, As the solder temperature increases during the warm-up phase of the cycle, it more readily deforms in response to the force exerted by the deflected lead; this produces a large shear strain in the +x direction (almost 3% in the first cycle as shown in Figure 4-7). In the subsequent cooling phase the solder again loses its ductility and yields only slightly in the reverse (-x) direction. After a number of cycles the lead achieves a deflection bias in the +x direction that provides a greater force in the yielding direction during the cold half cycle, and a reduced force during the hot half cycle. This equilibrium force offset is that required to provide equal horizontal creep strain in the plus and minus shear directions during each cycle; at this point the shear strain cycling becomes symmetrical, and the shear creep ratcheting equilibrates at a constant value. The number of cycles to achieve this symmetry is a function of the lead stiffness and lead-solder properties.

In response to this horizontal lead deflection offset that develops to maintain shear strain symmetry, out of phase tension-compression forces are developed normal to the board favoring tension creep in the solder joint for the case $\alpha_b > \alpha_p$, and compression creep in the solder joint for the case $\alpha_b < \alpha_p$. As a result, the tension-compression stress at the heel during the cooldown, "c-d-e", is significantly larger than the same stress during the warmup, "f-a-b", as shown in Figures 4-6 and 4-8, Consequently, a resultant creep-ratchet strain in the tension-compression direction is generated each cycle. Since normal-to-the-board tension drift has no means of generating a self-arresting force, it continues ratcheting at a constant rate as illustrated in Figure 4-2, For the opposite case ($\alpha_b < \alpha_p$), where normal-to-the-board ratcheting occurs in the compression direction, ratcheting will self arrest when the lead bottoms out against the solder pad.

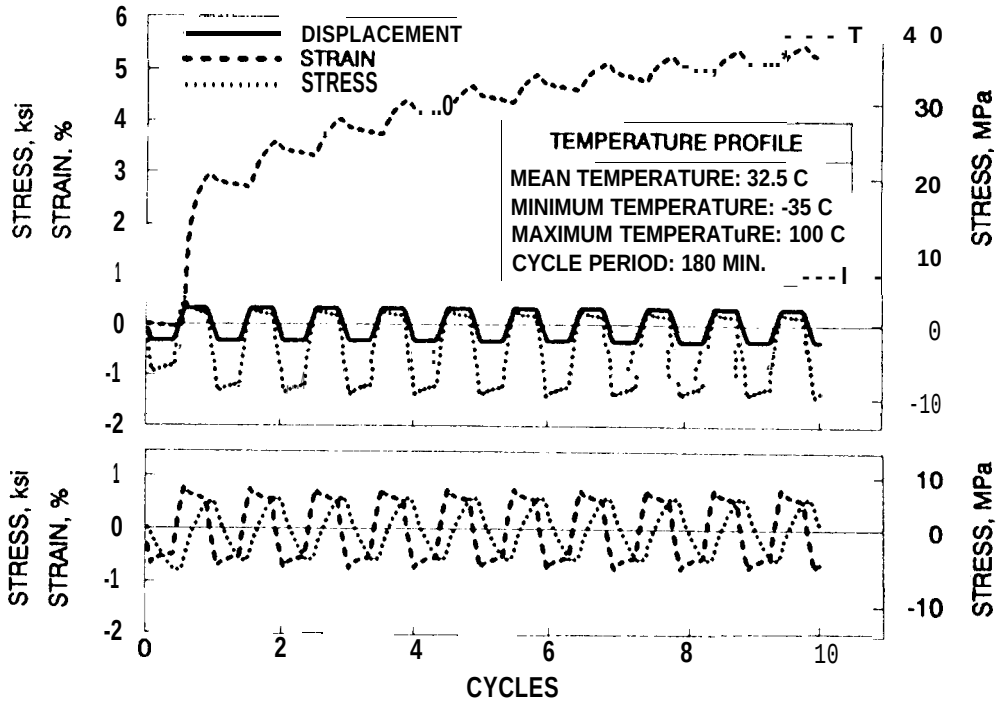

Fig, 4-7. **Transient shear stress and strain response to isothermal mechanical cycl ing (bottom) and thermal cycl ing (top) with identical displacement.**

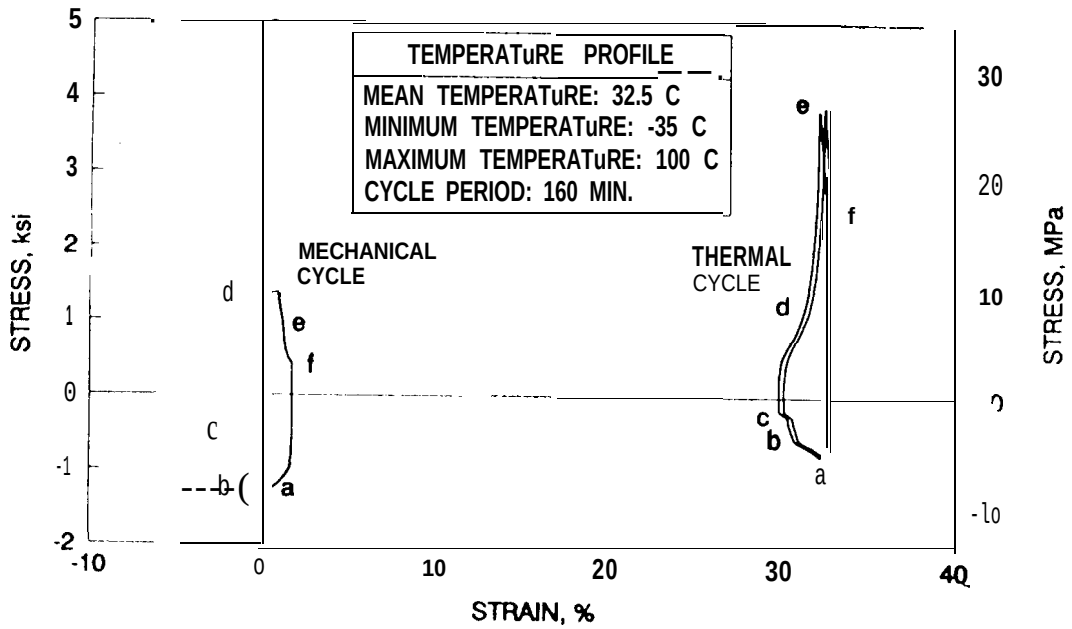

Fig. 4-8, Heel stress-strain hysteresis loops for thermally and mechanically strained solder joints.

Damage Prediction with Combined Creep Ratcheting and Fatigue

Before further examining the implications of the thermal-cycling strain simulation results it is useful to develop an analysis structure for comparing the damage caused by creep-ratcheting strain relative to that caused by cyclic fatigue strain.

Although there are many possible approaches to assessing the interactive damage contributions of creep rupture and fatigue, the most straightforward technique is to use Miner's Rule, which additively accumulates the individual fractional damage rates as follows:

$$\phi = \eta\, N/r + N/N_f = N(\eta/\Gamma + 1/N_f) \tag{15}$$

where

ϕ = fraction of useful service life consumed
η = creep ratchet strain per cycle
Γ = strain limit for creep rupture
N = number of cycles of applied stress
N_f = number of cycles to fatigue failure

Following our earlier lead, we use Manson's [9] fatigue relationship as embodied in Figure 2-1 to predict N_f, thus

$$N_f^{\beta}\, \Delta\epsilon = C \tag{16}$$

where

N_f = number of cycles to fatigue failure
$\Delta\epsilon$ = cyclic plastic strain range
$\beta \approx 0.40$
$C \approx 0.80$

To estimate the strain rupture limit (r), we again follow the lead of Manson, who in the development of his strain-cycle fatigue relationship (Equation 16), viewed the tensile test as a cyclic fatigue failure at 1/4 cycle. In a similar fashion, the strain range at the 1/4-cycle point on the Coffin-Manson plot can be taken as an rough estimate of the creep extension limit, i.e.

$$r \approx C/(0.25)^{\beta} \tag{17}$$

Combining Equations 15, 16, and 17 gives

$$\phi = N\,[\eta(0.25)^{\beta}/C + (\Delta\epsilon/C)^{1/\beta}] \tag{18}$$

Equation 18 can also be used to describe the acceleration of a particular test condition (1) over that of another condition (2) by noting that the acceleration ratio R is given by the ratio N_2/N_1, where N_1 is the number of environmental stress cycles of condition (1) required to yield the same damage as N_2 cycles of environmental stress condition (2), i.e., $R = N_2/N_1$ for $\phi_1 = \phi_2$; thus,

$$R = \frac{[\eta_1(0.25)^{\beta}/C + (\Delta\epsilon_1/C)^{1/\beta}]}{[\eta_2(0.25)^{\beta}/C + (\Delta\epsilon_2/C)^{1/\beta}]} \quad (19)$$

Returning to the above examples, Equation 18 can now be used to obtain an estimate of the relative importance of the observed strain ratcheting and cyclic fatigue.

With the modest 15°C-cycle depth used in Figure 4-2, recall that the creep ratcheting drifts were 2,5%, 0.5%, and 0.04% after 1000 cycles for the 10-, 20- and 30-mil lead heights, respectively, and the corresponding cyclic fatigue strain range per cycle was 0,62%, 0.16% and 0,051%, respectively, When these data and the parameters from Figure 2-1 are entered into Equation 18, the creep-ratchet and fatigue damage are found to be about equal in level.

Continuing this analysis for the simulation results of the deep 135°C thermal cycles provides the data assembled in Table 4-1. In the cases presented in Table 4-1, the dominating failure mechanisms are extension-compression low-cycle fatigue and creep at the heel (or toe) of the solder joints. Note that creep-ratcheting represents over 50% of the damage in most of the cases.

Table 4-1. Comparison of computed cyclic and creep-ratchet damage to solder joints on Flat-pak parts with different lead heights exposed to 15°C and 135°C thermal-cycle depths.

Lead Height mils (mm)	Cycle Depth (°C)	Cycle Strain Range %	% Creep Ratchet Strain per 1000 Cycles	Number of Cycles to Failure	Percent Damage due to Creep Ratchet	Accel. Factor 135°C to 15°C
10 (.25)	15	0.512	2,50	$2.9x10^4$	49	1
	135	4.630	683	152	69	195
20 (.51)	15	0.160	0.50	2.1X105	71	1
	135	2.830	330	347	76	618
30 (.76)	15	0.051	0.04	$2.6x10^6$	70	1
	135	1.470	9.13	4370	26	607

V. DISCUSSION AND CONCLUDING SUMMARY

It has been shown that the use of highly flexible leads can greatly reduce the strain developed in solder joints during cyclic loading conditions, The key requirement on the leads is to limit the maximum stress that is applied to the solder joint during peak loading conditions so as to minimize the generation of creep strain. For multi-hour loading dwells, such as is common for electronic assemblies that are power cycled daily (cars, computers, TVs), stress levels must be reduced significantly below the solder yield stress. Depending on the lead displacement applied by the part-board system, lead stiffnesses must generally be at least 1000 times more flexible than the solder itself (i.e. $\kappa < 10^{-3}$, as defined in Equation 10). Failure to use a sufficiently flexible lead may result in stresses that cause excessive creep-strain generation.

The rate at which solder creeps is a strong function of not only the applied stress, but also the solder temperature and metallurgical structure. As shown in Figures 2-4 and 2-5, temperature and solder aging conditions can have order-of-magnitude influences on creep-strain generation. The parametric studies presented provide an overview of the expected sensitivities to cycle rate, temperature, lead stiffness and thermal-cycle depth. When complex lead geometries such as gull wing leads are used, the type of loading (lateral shear versus normal-to-the-board tension-compression) is strongly dependent on the lead flexibility, Solder joints with leads having different compliance may result in different damage mechanisms in the same environment. For highly compliant leads, solder-joint failure is generally caused by tension-compression cyclic fatigue at the heel. However, for a very stiff lead, the dominant damage mechanism can be cyclic shear fatigue. When thermal cycling is introduced, even more complex behavior results from the strong creep-rate dependency on temperature. One such complexity is the development of creep ratcheting strains both parallel to, and normal to the board. This type of strain, which is not present in isothermal mechanical cycling, may represent 50% of the total damage associated with thermal cycling.

Because of unit-to-unit variabilities in solder joint geometry and aging condition, it is difficult to expect analytical simulation results to provide more than a qualitative feel for the important solder joint design parameters and their sensitivities. The ultimate verification of any given flexible lead design must be determined by test under conditions that accurately replicate the exact manufacturing processes and applicable loading conditions.

When viewing test results, it is important to note that the relative importance of each damage mechanism can change as time progresses. Initial shear creep ratcheting, if it does not exceed the rupture limit, is self-arresting after a few cycles. This damage mechanism can thus produce an early appearance of cracks, but does not necessarily result in crack propagation. Instead, as more and more cycles accumulate, the dominant damage mechanism can become tensile creep ratcheting and fatigue, eventually resulting in failure. An important observation is that conclusions based upon early test inspection, when one failure mechanism is predominant, may lead to erroneous projections

of failure at later times; this is because damage accumulation rates can change as different mechanisms become predominant.

Another important attribute of different lead configurations is their ability to fail gracefully with a large spread between the number of cycles for crack initiation and the number of cycles to electrical open circuit. The low toe stress with flexible gull-wing leads provides this desirable attribute and results in slow propagation of fatigue cracking down the solder side fillets. Measuring the length of cracking allows a useful quantification of the damage level accumulated to date, and the percent of useful life remaining in the joints.

Finally, where flexible leads are used for strain relief, it is critically important that the lead flexibility not be compromised (significantly stiffened) by subsequent manufacturing and assembly processes. Two such areas to watch carefully are: 1) the application of conformal coating and heat sink materials that can bridge the part-board gap and generate large normal-to-the-board stresses [30,31], and 2) the wicking of solder up into the lead system such that it significantly changes the bending stiffness of the leads. In a related problem, some ceramic J-lead parts that have body metallization very close to the "J" of the lead are vulnerable to soldering the flexible end of the lead to the bottom of the part. This "shorts out" the lead flexibility completely and can result in nearly immediate solder joint failure,

With properly designed flexible lead systems, solder strains will be substantially lower than with leadless devices, and completed boards should be capable of surviving hundreds of deep cyclic loads.

ACKNOWLEDGEMENT

The authors' contributions in this chapter were partially supported by the Jet Propulsion Laboratory, California Institute of Technology, under contract with the National Aeronautics and Space Administration. The authors would like to especially thank Ms. Elizabeth Jetter who conducted many of the computer simulations and generated most of the figures used in this chapter.

REFERENCES

1. Ross, R.G., Jr., et al., "Creep-Fatigue Interactions with F" exible Leaded Parts", ASME Paper No. 91-WA-EEP-27 presented at the 1991 ASME WAM, Atlanta GA, December 1991.

2. Ross, R.G., Jr., et al., "Creep-Fatigue Behavior of Micro-e" ectronic Solder Joints", Proceedings of the 1991 MRS Spring Meeting, Anaheim CA, April 30 - May 4, 1991.

3. Lau, J,H., Solder Joint Reliability: Theory and Application, Van Nostrand Reinhold, New York, 1991.

4. Frear, D.R., Jones, W.B. and Kinsman, K.R., Solder Mechanics: A State of the Art Assessment, Minerals, Metals and Materials Society, Warrendale PA, 1991.

5. Aldrich, J. W. and Avery, D. H., "Alternating Strain Behavior of a Superplastic Metal," in Ultrafine Grain Metals, Proceedings of the 16th Sagamore Army Material Research Conference, Aug. 1969, Syracuse University Press, 1970, pp.397-416.

6. Wild, R. N., "Some Fatigue Properties of Solders and Solder Joints," IBM Report No. 7AZOO0481, IBM Federal Systems Division, New York, 1975.

7. Solomon, H. D., "Influence of Temperature on the Fatigue of CC/PWB Joints, " Journal of the IES, January/February 1990, pp. 17-25.

8. Manson, S.S., "Effect of Mean Stress and Strain on Cyclic Life," Machine Design, August 1960, pp. 129-135.

9. Manson, S.S., "Fatigue: A Complex Subject-- Some Simple Approximations," Engineering Mechanics, Vol. 5, 1965, pp. 193-226.

10. Solomon, H.D., "Predicting Thermal and Mechanical Fatigue Lifes from Isothermal Low-cycle Data", Solder Joint Reliability: Theory and Application, Van Nostrand Reinhold, New York, 1991, pp. 406-454.

11. Solomon, H.D., ASME J. of Electronic Packaging, v. 111, 1989, pp. 75-82,

12. Vaynman, S., Fine, M.E., and Jeannotte, D.A., "Low-cycle Isothermal Fatigue Life of Soldered Materials," Solder Mechanics, Edited by Frear, D. R., et al, The Minerals, Metals & Materials Society, 1991, pp. 333-360.

13. Gohn, G.R. and Ellis, W.C., Proc. ASTM, v. 51, 1951, pp. 721-740.

14. Solomon H.D., Electronic Packaging Materials and Processes, Ed. J.A. Sortel 1 ASM, 1985, pp. 29-49.

15. Solomon H.D., IEEE 38th Electronic Components Conf., May 1988, pp.7-13.

16. Engelmaier, W., "Functional Cycling and Surface Mounting Attachment Reliability", ISHM Technical Monographic Series 6984-002, International Sot. for Hybrid Microelectronics, 1984, pp. 87-114.

17. Engelmaier, W., Circuit World, v. 11, no, 3, 1985, pp. 61-67.

18. Engelmaier, W., "Solder Attachment Reliability, Accelerated Testing, and Result Evaluation", Solder Joint Reliability: Theory and Application, Van Nostrand Reinhold, New York, 1991, pp. 545-587.

19. Pan, T-Y., "Thermal Cycling Induced Plastic Deformation in Solder Joints--Part 1: Accumulated Deformation in Surface Mount Joints", ASME Journal of Electronic Packaging, Vol. 113, March 1991, pp. 8-15.

20. Cline, H. E. and Alden, T. H., "Rate Sensitive Deformation in Tin-Lead Alloy," Trans. AIME, vol. 239, 1967, pp. 710-714,

21. Zehr, S.W. and Backofen, W,A., "Superplasticity in Lead-Tin Alloys", Transaction of the ASM, v.61, 1968, pp. 300-312.

22, Guo, Z., Sprecher, A.F. and Conrad, H., "Plastic Deformation Kinetics of Eutectic Pb-Sn Solder Joints in Monotonic Loading and Low-cycle Fatigue", ASME Paper No. 91-WA-EEP-48 presented at the 1991 ASME WAM, Atlanta GA, December 1991.

23. Weinbel, R.C., Tien, J.K., Pollak, R.A., and Kang, S.K., "Creep-Fatigue Interaction in Eutectic Lead-Tin Solder Alloy", J. of Material Science. Letter, v.6, 1987, pp. 3091-3096.

24. Avery, D.H. and Backofen, W.A., "A Structural Basis for Superplasticity," Transactions of the ASM, v.58, 1965, pp. 551-562.

25. Murty, G.S., "Stress Relaxation in Superplastic Materials", J. of Material Science, v.8, 1973, pp. 611-614.

26. Kashyap, B.P. and Murty, G.S., "Experimental Constitutive Relations for the High Temperature Deformation of a Pb-Sn Eutectic Alloy", Materials-Science and Engrg, v.50, 1981, pp. 205-213.

27, Arrowood, R., Mukherjee, A. and Jones, W.B., "Hot Deformation of Two-phase Mixtures", Solder Mechanics: A State of the Art Assessment, Minerals, Metals and Materials Society, Warrendale PA, 1991, pp. 107-153.

28. Lampe, B.T., "Room Temperature Aging Properties of Some Solder Alloys", Welding Research Supplement, October 1976, pp. 330-340.

29. NASA, "Requirements for Soldered Electrical Connections," NHB 5300.4(3A-1), revalidation date June 1986.

30, Ross, R.G., Jr., Magellan/Galileo Solder Joint Failure Analysis and Recommendations, JPL Publication 89-35, Jet Propulsion Laboratory, Pasadena, California, September 1989.

31. Ross, R.G., Jr., "A Systems Approach to Solder Joint Fatigue in Spacecraft Electronic Packaging," ASME Journal of Electronic Packaging, Vol. 113, June 1991, pp. 121-128,

FIGURE CAPTIONS

Fig. 1-1. Typical flexible lead geometries found on surface-mount electronic components: (a) Flat-pak with gull-wing leads, (b) Plastic leaded chip carrier (PLCC) with J-leads, (c) DIP with gull-wing leads, and (d) Quad Flat-pak with fine-pitch gull-wing leads.

Fig. 2-1, Coffin-Manson curves fitted to typical eutectic Sn-Pb solder fatigue data from Aldrich [5], Wild [6], and Solomon [7].

Fig. 2-2. Effect of definition-of-failure on slope of Coffin-Manson fatigue curves (from Solomon [11]).

Fig. 2-3. Dependence of fatigue life of 60-40 Sn-Pb solder on loading frequency as measured by various investigators [10,14,15].

Fig. 2-4. Dependence of strain-rate on applied stress and metallurgical condition of room-temperature eutectic Sn-Pb solder.

Fig. 2-5. Dependence of strain-rate on applied stress and temperature for eutectic Sn-Pb solder (from Cline and Alden [20]).

Fig. 2-6. SEM back-scatter photographs (tin is dark region) showing cross-sections of typical gull-wing flat-pak solder joints taken from spacecraft electronics with the indicated aging histories (From Ross, et al. [2]).

Fig. 3-1. Schematic of single-node solder element with series spring representing the combined elastic flexibility of the solder and electronic component lead.

Fig. 3-2, Creep-relaxation response of solder as a function of relative spring stiffness (κ) for a fixed initial loading stress of 1 ksi,

Fig. 3-3. Creep-relaxation response of solder as a function of relative spring stiffness (κ) for a fixed spring-tip displacement (Ax) corresponding to a 10% strain upon complete stress relaxation,

Fig, 3-4. Creep-relaxation Master Curves that describe creep-relaxation response of solder as a function of relative spring stiffness (κ) for initial stress (σ_o) or a spring-tip displacement (Ax) corresponding to a final strain (ϵ_f) upon complete stress relaxation.

Fig. 3-5. Effect of cyclic frequency of loading and relative spring stiffness (κ) on computed solder strain range.

Fig. 3-6, Effect of solder temperature and relative spring stiffness (κ) on computed solder strain range.

Fig. 3-7. Cyclic displacement profile (Ax versus time) used for isothermal strain studies with single-node spring-loaded solder element.

TABLE OF CONTENTS

AUTHOR BIOGRAPHIES

Ronald G. Ross, Jr. - Supervisor, Thermal and Cryogenics Technology Group - Jet Propulsion Laboratory, Pasadena, California. Dr. Ross, in addition to his broader management responsibilities, heads JPL's Reliability Physics Research directed at developing NASA design guidelines and test standards for solder attachment of surface-mount electronic components. Over the past 20 years he has conducted extensive research in the fields of reliability, life prediction and qualification of semiconductor products. He has authored or co-authored over 100 publications covering his research, and is JPL's key trouble shooter for solder related failures. He received his PhD from the University of California at Berkeley in 1968, specializing in mechanical design and finite element structural modeling. He is a member of Tau Beta Pi, Pi Tau Sigma and Sigma Xi Honor Societies.

Liang-chi Wen - Member of Technical Staff, Thermal and Cryogenic Technology Group, Jet Propulsion laboratory, Pasadena, California. Dr. Wen is a senior researcher with emphasis in modeling the thermal-mechanical response and degradation dynamics of high reliability spacecraft systems. lie has been working in the field of reliability physics and thermal-mechanical modeling since 1969. He received his Ph.D. from Purdue University in 1968.